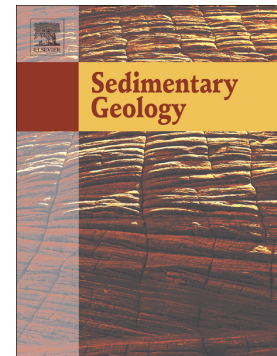


Accepted Manuscript

The influence of intrabasinal tectonics in the stratigraphic evolution of piggyback basin fills: Towards a model from the Tremp-Graus-Ainsa Basin (South-Pyrenean Zone, Spain)

Emmanuelle Chanvry, Rémy Deschamps, Philippe Joseph, Cai Puigdefàbregas, Miquel Poyatos-Moré, Josep Serra Kiel, Daniel Garcia, Stéphane Teinturier



PII: S0037-0738(18)30221-5
DOI: doi:[10.1016/j.sedgeo.2018.09.007](https://doi.org/10.1016/j.sedgeo.2018.09.007)
Reference: SEDGEO 5397
To appear in: *Sedimentary Geology*
Received date: 28 June 2018
Revised date: 19 September 2018
Accepted date: 20 September 2018

Please cite this article as: Emmanuelle Chanvry, Rémy Deschamps, Philippe Joseph, Cai Puigdefàbregas, Miquel Poyatos-Moré, Josep Serra Kiel, Daniel Garcia, Stéphane Teinturier , The influence of intrabasinal tectonics in the stratigraphic evolution of piggyback basin fills: Towards a model from the Tremp-Graus-Ainsa Basin (South-Pyrenean Zone, Spain). *Sedgeo* (2018), doi:[10.1016/j.sedgeo.2018.09.007](https://doi.org/10.1016/j.sedgeo.2018.09.007)

This is a PDF file of an unedited manuscript that has been accepted for publication. As a service to our customers we are providing this early version of the manuscript. The manuscript will undergo copyediting, typesetting, and review of the resulting proof before it is published in its final form. Please note that during the production process errors may be discovered which could affect the content, and all legal disclaimers that apply to the journal pertain.

The influence of intrabasinal tectonics in the stratigraphic evolution of piggyback basin fills: towards a model from the Tremp-Graus-Ainsa Basin (South-Pyrenean Zone, Spain)

Emmanuelle Chanvry ^{a, b, c*}, Rémy Deschamps ^b, Philippe Joseph ^b, Cai Puigdefàbregas ^d, Miquel Poyatos-Moré ^e, Josep Serra Kiel ^f, Daniel Garcia ^c, Stéphane Teinturier ^a

^a TOTAL SA, CSTJF, avenue Larribau, 64018 Pau, France.

^b IFP Énergies nouvelles, 1 et 4 avenue de Bois-Préau, 92852 Rueil-Malmaison, France.

^c Centre SPIN, Ecole Nationale Supérieure des Mines de Saint Etienne, and UMR CNRS 5600, 158 cours Fauriel, 42023 Saint-Etienne, France ;

^d Departamento de Geodinámica i Geofísica, Faculta de Geologia, Universitat de Barcelona (UB), Carrera de Martí i Franquès, s/n, 08028 Barcelona, Spain.

^e Department of Geosciences, University of Oslo, Sem Saelands vei 1, 0371 Oslo, Norway.

^f Departamento d'Estratigrafia, Paleontologia i Geociències Marines, Faculta de Geologia, Universitat de Barcelona (UB), Carrera de Martí i Franquès, s/n, 08028 Barcelona, Spain.

*Corresponding author. E-mail address: emmanuelle.chanvry@hotmail.fr (E. Chanvry).

Abstract

Piggyback basins often display asymmetric sedimentary successions influenced by both regional and local syn-depositional tectonic structures. There are few examples where a complete exhumed piggyback basin fill can be analyzed, from proximal, close to source areas, to the distal deep-water sinks. The study of these basins is key to extract the stratigraphic signal of intrabasinal tectonics, which often competes and can even overprint other controlling factors such as eustasy, climate, or autogenic processes. The purpose of this paper is to propose a more detailed model of the evolution of piggyback basin fills, which recognizes the influence of intrabasinal tectonic activity, specific to the piggyback context and the resulting stratigraphic architecture. We investigate the Tremp-Graus-Ainsa piggyback basin, located in the southern Pyrenees, during early

Eocene, which was influenced by the development of the Montsec frontal thrust. Twenty four stratigraphic sections, totaling 14 km of logged thickness, are analyzed, covering 60 km of the basin. The stratigraphic surfaces have been correlated in order to define large-scale stratigraphic units and a new sequence stratigraphic framework. The influence of local tectonics in the basin record is identified by abrupt lateral sediment thickness variations, abrupt changes of depositional environments, local erosion surfaces, and changes in dominant sedimentary process regimes and paleocurrent directions through space and time. As a result, we propose a new tectono-stratigraphic model for the development of the Tremp-Graus-Ainsa Basin. Specifically, we identify (1) an underfilled stage with initial high flexural subsidence and a frontal subaqueous blind anticline thrust propagation that controls a dominantly carbonate environment, followed by a progressive increase in siliciclastic sediment supply, and (2) an overfilled stage with an increase in frontal thrust propagation causing new emergent sediment sources. This second stage evolves from an active emerged blind anticline thrust to a migrating thrust that moved along lateral ramps, and which caused the decoupling of the Tremp-Graus uplifted wedge-top sub-basin from the Ainsa subsiding foredeep domain. Finally, we provide a new model intrinsic to the piggyback basin development with four main stages, controlled by changes in intrabasinal tectonic activity, flexural subsidence and orogeny axial zone evolution, which ultimately modulate sediment supply and creation and distribution of accommodation space.

Keywords: Piggyback basin, intrabasinal tectonic controls, basin-scale correlation, stratigraphic record, Tremp-Graus-Ainsa Basin, South-Pyrenean foreland basin

1. Introduction

Piggyback basins, included in the wedge-top-depozone within a foreland system (DeCelles and Giles, 1996), are basins that form and are filled while being carried on top of thrust sheets (Ori and Friend, 1984). They therefore represent a powerful tool to constraint the timing of foreland and fold-thrust-belt deformations. With the aim to reconstruct tectonic kinematics, many works in piggyback basin fills focus on the impact of thrust activity in basin sedimentation recorded by widespread angular unconformities, depocentre migration, development of growth strata, onlap terminations and truncations against growing structures, or development of syntectonic progressive unconformities (e.g., Riba, 1976; Anadón et al., 1986; Burbank and Beck, 1989; Roure et al., 1989; Zoetemeijer et al., 1993; Baby et al., 1995; Zapata and Allmendinger, 1996; Mugnier et al., 1997; Bonini et al., 1999; Marzo and Steel, 2000; Clevis et al., 2004; Ford, 2004; Charreau et al., 2008; Roure, 2008). In a similar perspective, the interaction between compressive structures, drainage patterns and fluvial architecture in piggyback contexts is also relatively well studied (e.g., Friend et al., 1986; Bentham and Burbank, 1996; Ramos et al., 2002; Bès de Berc et al., 2005; Morley and Leong, 2008; Vergés, 2009; Bonorino and del Valle Abascal, 2012). The piggyback basin stages are mostly summarized and grouped as one, often a single event in the complete evolution of a foreland succession, and hence studies of their sedimentary fill are often not very detailed (Cipollari and Cosentino, 1995; Pivnik and Khan, 1996; Hermoza et al., 2005). As an example, regional-scale piggyback basin studies usually consider only two major changes in basin fill dynamics, commonly described as (1) marine / undersupplied / transgressive stage, followed by a (2) continental / oversupplied / regressive stage that are considered to be mainly controlled by the development of regional / local syn-

depositional tectonic structures, or by the setting and erosion of new thrust sheets (Ferrière et al., 1998, 2004; Evans and Elliott, 1999; Martín-Martín and Martín-Algarra, 2002; Rossi et al., 2002; Chiang et al., 2004; Conti et al., 2008; Maestro, 2008; Gugliotta, 2012; Gugliotta and Morticelli, 2012; Suriano et al., 2015). These two oversimplified stages appear in most of piggyback basin reconstructions, which are often based on detailed studies of discrete segments of the basin. Thus, a refinement of model that concerns the development of a single piggyback basin formed in the hanging wall of one frontal thrust is needed, in order to differentiate higher-frequency tectonic events specific and inherent to the piggyback context in the coeval sedimentary record during the complete piggyback sequence. This differentiation is often challenging because the piggyback basin infill is also the result of a complex interaction and competition between (a) allogenic controlling factors acting at a regional scale (i.e., eustasy, climate, load-driven subsidence, isostatic rebound and regional uplift linked to the fold-thrust belt and associated foreland system tectonic context); (b) the local influence of autogenic forcing in each depositional system considered, and (c) the local intrabasinal tectonic controls specific to the piggyback basin activity (Lawton and Trexler, 1991; Talling et al., 1995; DeCelles and Giles, 1996; Nijman, 1998) (Fig. 1). One way to unravel the impact of controlling factors (regional tectonic, climate, eustasy) in basin architecture and sedimentation may be to extract the signal specific to the internal piggyback tectonics. The main objective of this paper is therefore to study and define a typical stratigraphic sequence of a piggyback basin infill, from the early stages of the frontal thrust development to the late stage with piggyback transport caused by the thrust displacement. The Tresp-Graus-Ainsa Basin (Southern Pyrenees) during the early Eocene is particularly relevant due to the excellent outcrop conditions of the

complete exhumed piggyback basin fill, from proximal depositional systems close to the source areas to the distal deep-water sinks. This allows identification of large-scale cycles that are related to major tectonic phases (Garrido-Megias, 1973; Nijman and Nio, 1975; Puigdefàbregas and Souquet, 1986; Nijman, 1998; Remacha and Fernández, 2003) and in which the relative contribution of climate and eustasy is still a matter of debate (Peper and de Boer, 1995; Weltje et al., 1996; Nijman, 1998; Schmitz and Pujalte, 2003; Pickering and Bayliss, 2009; Castelltort et al., 2017). With the aim to study the specific impact of intrabasinal tectonic controls on sedimentation during an entire thrust-sheet emplacement period/sequence, we investigated the early Eocene series corresponding to a single major tectonic event related to the emplacement and development of the Montsec frontal thrust. By comparison and discussion of this study with other piggyback basin successions, we attempt to propose a conceptual model of a piggyback basin infill, specific to piggyback basin emplacement.

2. Geological setting

2.1. Structural framework

The Pyrenean mountain belt is the result of the continental collision and subsequent subduction of the Iberian plate under the Eurasian plate, which took place from the upper Cretaceous to the early Miocene. At a crustal scale, this deformation implied Hercynian basement thrust sheets that formed a south-directed central sheet duplex (Muñoz, 1992) (present-day Axial Zone; Fig 2a, d), and the South Pyrenean Central Unit (hereinafter referred to as SPCU; Séguret, 1972). This unit corresponds to a set of allochthonous thrust sheets of Mesozoic and Cenozoic basins developed in a piggyback sequence upon and in front of three major thrusts (Bóixols, Montsec and Sierras Marginales thrusts; Fig. 2d) branching in the Triassic decoupling level (Choukroune et

al., 1968; Séguret, 1972; Muñoz, 1992; Puigdefàbregas et al., 1992). The Bóixols Thrust (Fig. 2b, d) is generated by the inversion of pre-existing Mesozoic East-West oriented normal faults (Roure et al., 1989; Bond and McClay, 1995) during the upper Cretaceous (Santonian) and sealed by the Maastrichtian (Ardèvol et al., 2000) (Fig. 2c, d). The Bóixols Thrust, emplaced during the upper Cretaceous, delimits the Organyà-La Pobla (hanging wall) and the Tremp-Graus sub-basins (footwall) (Roure et al., 1989; Berastegui et al., 1990; Bond and McClay, 1995; Ardèvol et al., 2000; García Senz, 2002) (Fig. 2c, d). The Montsec Thrust, which presently separates the Tremp-Graus and the Àger sub-basins (Fig. 2b, d) was active during the Paleocene-early Eocene (Teixell and Muñoz, 2000; Muñoz et al., 2013) (Fig. 2c, d). The Sierras Marginales Thrust forms the boundary between the Àger basin and the present-day Ebro Foreland Basin, and was active during the mid-Eocene (Lutetian) - Oligocene (Fernández et al., 2012) (Fig. 2c, d). The SPCU is bounded to the north by the Morerres backthrust (Fig. 2b), a passive roof thrust related to the piling up of the Hercynian basement thrust sheets of the Axial Zone (Weltje et al., 1996; Vincent, 2001; Whitchurch et al., 2011). The eastern boundary of the SPCU (and of the Tremp-Graus sub-basin) is formed by the lateral ramp system of the Segre Fault (Vergés, 2003) (Fig. 2b). The position and nature of the western boundary of the Tremp-Graus sub-basin varies slightly according to several authors, but it is mostly placed coinciding with the eastern part of the Ainsa sub-basin (Nijman and Nio, 1975; Mutti et al., 1988; Barnolas, 1992; Anastasio et al., 1992; Soto et al., 2002; Fernández et al., 2004, 2012; Muñoz et al., 2013).

2.2. The Tremp-Graus and Ainsa sub-basins

During Ypresian times, the Tremp-Graus sub-basin was an East-West elongated basin controlled southward by the emplacement of the Montsec Thrust (Fig. 2c). Continental

to shallow marine sedimentary systems evolved to basinal environments towards the West into the Ainsa and Jaca sub-basins, and opened into the ocean at the Bay of Biscay (Plaziat, 1981). The transition from shallow to deep-water systems is observed in the Ainsa sub-basin, where synsedimentary NNW-SSE oriented structures, included in La Fueba Thrust System, were active during the Ypresian as the Arro, Los Molinos, Atiart and Ferrera Thrusts (Barnolas et al., 1991; Martínez-Peña, 1991; Casas et al., 2002; Fernández et al., 2012; Muñoz et al., 2013) (Figs. 3, 4). This system corresponds to the oblique lateral ramp linking the Montsec thrust to the Peña Montañesa thrust (Muñoz et al., 2013). Farther east, the NNE – SSE Foradada Fault is a tear fault located in the hanging wall of the Montsec thrust, and was active during the upper Ypresian (Cuisian) and Lutetian (Fernández et al., 2012). The northern part of the Tremp-Graus sub-basin in its central sector is affected by the Turbón structure, which was interpreted by López-Blanco et al. (2003) as a blind thrust, generated by the inversion of a upper Cretaceous structure which became a positive relief during southward transport by the Montsec thrust from the lower Ypresian (Ilerdian) to the upper Ypresian (Cuisian; Fig. 3). This interpretation may be transposed to the Coll del Vent Anticline (Vincent, 2001) and the Roda fold system (García Senz, 2002; López-Blanco et al., 2003) (Fig. 3).

2.3. Lithostratigraphy

The Tremp-Graus sub-basin fill corresponds to an approximately 7 km-thick syn-orogenic sedimentary succession spanning from the Upper Cretaceous to Oligocene. The succession shows continental alluvial to deep marine environments, with different deepening and shallowing upward cycles controlled by the activity of different thrust sheets (Fig. 2c). In this paper, we focus on the Paleocene-lower Eocene interval, which is related to the Montsec thrust activity. The Paleocene-lower Eocene succession has

been divided into four main groups (Fig. 4): (1) Tremp Group (Paleocene) (Fonnesu, 1984; Mutti et al., 1988), (2) Alveolina Limestone (lower Ypresian; lower Ilerdian) (Fonnesu, 1984; Mutti et al., 1988; Serra-Kiel et al., 1994) or Ager Sequence (Eichenseer and Luterbacher, 1992; Baceta et al., 2011); (3) Figols Group (lower Ypresian to middle Ypresian; middle Ilerdian to lower Cuisian) (Mutti et al., 1988) or Llimiana, Alinya and Oden Sequences (Eichenseer and Luterbacher, 1992; Baceta et al., 2011); and (4) Montañana Group (middle Ypresian; lower Cuisian to Lutetian) (Nijman, 1998). A more detailed lithostratigraphic synthesis is given in Table 1 with the age of the Formation through the Tremp-Graus-Ainsa Basin. The transition between the Tremp-Graus and Ainsa sub-basins is characterized by submarine canyon incisions (Mutti et al., 1988; Muñoz et al., 1994; Casas et al., 2002; Poyatos-Moré, 2014). Some of these are contemporaneous with the lower Eocene studied succession. The Atiart surface (Fig. 4) is dated as early-middle Cuisian (Muñoz et al., 2013; Poyatos-Moré, 2014), and is developed between the Foradada fault and the Atiart thrust (Fig. 3) whereas the Charo-Lascorz surface (Fig. 4) is dated as latest Cuisian in age (Payros et al., 2009; Muñoz et al., 2013; Poyatos-Moré, 2014).

3. Dataset and methods

3.1. Lithological successions

The dataset consists of twenty-four sedimentological field sections (Fig. 3), logged at 1/200 scale for a total of ca. 14 km of measured vertical section. Detailed information is presented in Appendix A which indicates field section name, abbreviation, and location with GPS coordinates. The sedimentary succession is exposed along a large East-West syncline and covers a distance of 75 km from East to West (Fig. 3). Four regional reference sections from the Paleocene to the late Ypresian (Cuisian) form the main

chrono- and lithostratigraphic framework to study the Ypresian succession (South Ribagorzana, Montanana, Isabena and Campo sections; Fig. 3). The measured sections are located mainly on the northern flank of the Tremp syncline, except in the eastern part of the basin, where a section is made on the southern flank (Sr section, Fig. 3). The North-South syndimentary wedge geometry can be roughly recognized by the Isbena, Montanana and South Ribagorzana sections (Fig. 3). Despite the lack of continuous outcrops in a N-S direction and the distance between sections (ranging from 10^2 - 10^4 m), local observations and previous works based on seismic sections (López-Blanco et al., 2003), field data (Nijman, 1998) and analysis of aerial photos (see Sgavetti, 1992) are used to complete physical correlation of stratigraphic surfaces.

3.2. Method for stratigraphic correlation

The high resolution stratigraphic framework is based on the application of classical sequence stratigraphy principles to sedimentary facies and stacking pattern analysis along the measured stratigraphic sections. Facies are defined by grain-size, texture, sorting, sedimentary structures, fauna, non-fauna content, bioturbation intensity and are grouped into facies associations (FA), from which depositional environments are interpreted. One hundred and twenty thin sections were used to accurately identify sedimentary facies and determine microfaunal species. Seventeen facies associations (FA) are recognized (FA1 to FA17). Different basin scale oriented depositional systems are reconstructed and correspond to an assemblage of genetically-linked depositional environments, which pass vertically and laterally into each other through the basin. These systems are linked to each other in order to propose an evolutionary model with the aim to recreate a general and predictable distal-proximal depositional profile typical at piggyback basins.

Analysis of stacking patterns along sections according to this general profile allows us to recognize (1) shallowing trends, and (2) deepening trends characterized by landward retreat. Shallowing to deepening upward trends are delimited by a transgressive surface (Catuneanu et al., 2009) that is located at the maximum of deltaic or carbonate platform progradation in littoral domains and by mottled top of fluvial channels due to major paleosol development in continental domains. The maximum flooding surface (Van Wagoner et al., 1988) is placed at the hinge (interval or surface) between a deepening and shallowing trend and at the maximum preservation of floodplain deposits without paleosol development in continental domains. Shallowing trends can also include subaerial unconformities (Catuneanu et al., 2009), characterized by the development of a major erosional surface (sequence boundary; Van Wagoner, 1988) in continental domains with an increase in fluvial channel incision/amalgamation or grain size. In coastal domains, the subaerial unconformity (corresponding to the correlative conformity from Catuneanu et al., 2009) may show an abrupt basinward shift of depositional environments.

4. Results

4.1. Facies model

4.1.1. Facies associations and depositional environments

The Tresp-Graus-Ainsa Basin is characterized by mixed clastic-carbonate deposits covering a full range of depositional environments. Detailed facies analysis was used to define seventeen facies associations (FA) ranging from continental to deep marine domains that are detailed in the following section and summarized in Figures 5 and 6.

Alluvial fan (FA1)

This FA is made of poorly sorted and sub-rounded partly stratified pebbles and cobbles conglomerate supported by a coarse-grained sandstone matrix. The basal surface is erosive and shows 10 to 20 cm wide scours marks and lag deposits with cobble to boulder clasts. This facies is intercalated with 0.5 to 1 m thick, medium to very coarse-grained poorly sorted through cross-bedded sandstones with scattered plant debris. The succession from the conglomerates to medium grained intercalated sandstones is organized in a transitional fining upward trend (Fig. 6a). The top of the sandstone is sharp and eroded by the followed conglomeratic level. This FA is 1 to 10 m thick and commonly amalgamated with a 100 m to 1 km wide lateral extent.

The conglomerates record high amplitude mass-flows deposited from hyper-concentrated high-density gravity flash-discharge events (Miall, 1993; Sohn et al., 1999). Sandstone intercalations indicate more diluted unidirectional transport from stream flow processes occurring during the waning stage of major flash-flood events. This FA is interpreted as proximal braided streams or stream-flow dominated alluvial fans (Galloway and Hobday, 1996).

Braided channel (FA2)

This FA shows very coarse to medium poorly sorted sandstones with floating pebbles evolving upwards to plane parallel laminations in a fining upward trend (Fig. 6b). Interstratified tabular to tangential cross-bedding sets are also observed in this facies with 0.5 to 1.5 m thick in average. Plant debris is present. The base of this FA is erosive with lag deposits or local crudely stratified conglomeratic base with 5 to 10 cm wide scours marks. The top of the FA is occasionally mottled by rootlets. The mean thickness of the isolated bodies is of 1 to 2 m but can reach a maximum thickness of 15-20 m in

case of amalgamation. The lateral extension varies from 5m to 2-3 km when channel are highly amalgamated.

This FA is interpreted as the development of a multistorey braided channel network developed during high discharge flooding events (Williams and Rust, 1969) allowing for the migration of transverse and longitudinal bars (Miall, 1977; Cant and Walker, 1978; Ramos and Sopena, 1983; Bridge, 1993). Channel abandonment during low water stage is marked by the development of a paleosol on fine grained mottled material. According to the nomenclature of Huerta et al. (2011) (W/T ratio, sand connectivity and floodplain preservation potential), three types of braided channels were identified (Fig. 5): (1) multistorey braided belt channels (FA2.1), (2) intermediate sheet-like bodies (FA 2.2), and (3) ribbon channels (FA 2.3).

Meandering Channel (FA3)

This FA shows an overall fining upward sequence passing from trough cross-bedded coarse to medium sandstone, with an erosive scoured base, to heterolithic facies with fine rippled sandstones alternating with silty-claystones. Bedset are 5 to 50 cm thick and organized in inclined (15-20°) sets marked by thickening upward clayey drapes from 1 to 20 cm (Fig. 6c). On the top, 2 to 5 cm wavelength current ripples show a current direction perpendicular to the dip of the inclined bed set. 0.5 to 1 m thick clay plugs and rootlets occur at the top of the channel fill. The thickness of this facies association is about 2 to 30 m and the lateral extension can reach 50 m.

The inclined bedding is interpreted as lateral accretions surfaces dipping towards the channel axis and indicates high sinuosity meandering channel processes (Leeder and Alexander, 1987; Odgaard, 1989) and meander cut-off during with flood discharge (Puigdefabregas and Van Vliet, 1977).

Floodplain deposits (FA4)

This FA shows brownish to reddish horizontal plane-parallel silty claystone deposits including 0.5 to 1 cm thick carbonate concretions and pedogenic mottled horizons on 0.5 to 1 m in thickness. Decimeter thick rippled very fine to fine-grained non-erosive sandstone beds of limited lateral extent (2 to 5 m) are also observed, as well as 0.5 to 1.5 m thick mottled siltstone that reaches a minimum widths of about 50 m.

The silty claystone material indicates lower flow conditions allowing for suspension fall out in backwater during channel abandonment (Smith et al., 1989). The sediments are later modified by pedogenic processes. The color changes reflect variations in redox conditions during water table fluctuations (Foix et al., 2013). The sandstones are interpreted as channel overbank or crevasse-splay deposits (Allen, 1963, 1965; Miall, 1996; O'Brien and Wells, 1986; Kraus, 1987; Bown and Kraus, 1987).

Fluvial-dominated delta plain (FA5)

This FA consists of 1 to 3 m thick, fining-upward trough cross-bedded very coarse to medium-grained poorly sorted sandstone evolving upwards to climbing ripples and oyster and gastropod-rich silty-clayey facies (Fig. 6d) organized in a 0.5 to 1.5 m thick bedset. Shell fragments, Ophiomorpha burrows and plant debris are also observed. The base is erosive with a slightly concave up shape (generally less than 2 m in strike section) showing scours marks and lag deposits including oyster shell fragments and mudclasts. This facies association ranging from 3 to 20 m wide.

This FA is interpreted as subaqueous distributary channels formed by channelized bedload process during waning stage of river flood events in a coastal domain as suggested by the fauna and burrows.

Bay environment (FA6)

This FA is composed of bluish gray silty claystone including well preserved oligospecific fauna like oysters, cerithids and *Pectens*. *Cruziana*, *Ophiomorpha* ichnofacies are observed. Locally, sandstone beds show three specific patterns: (1) erosive 0.5 to 1.5 m thick fining-upward muddy sandstones with scattered medium to coarse grains including faunal accumulation; (2) 10 to 30 cm thick beds of medium-grained sandstones with sigmoidal cross stratification, clay drapes and mudclast, and (3) 0.2 to 1 m thick coarsening and thickening upward fine to medium grained rippled and cross laminated sandstones with abundant plants debris and mudclasts.

This muddy dominated environment indicates suspension fall-out in a quiet environment. Fauna-rich fine-grained sandstone beds are interpreted as storm deposits during transgressive events (Lafont, 1994). The sigmoidal cross-stratified sandstone beds indicate tidal deposits. The coarsening upward climbing rippled sandstones are interpreted as crevasse splay deposits. Oligospecific faunal assemblage suggests the deposition in a brackish, low oxygenate, and nutrient-rich bay or restricted lagoon environment with a variable salinity (Luterbacher, 1970; Pemberton, 1992; Gertsch et al., 2010), related locally to tide, fluvial or storm events.

Tidal channel (FA7)

This FA shows inclined and laterally accreted 20 cm thick in average bedsets of coarse to medium grained sandstones, rhythmically draped by 2 to 10 cm thick silty clays (Fig. 6e). These sandstones are rich in broken mollusk shells and *Skolithos* to *Thalassinoides* ichnofacies. Megaripples and sigmoidal bedsets with 0.5 to 1 cm thick mud drapes are observed with a current direction perpendicular to the main accretion dip and are followed by reverse current ripples. This facies evolves upwards to clayey facies showing 1 to 3 cm flaser bedding in fine to medium-grained sandstones. The basal

surface is erosive, with a pebble lag deposits and large amounts of mudclasts and plant debris. This facies association ranging from 2 to 5 m thick.

This FA shows strong evidences for tidal influence (Shanley et al., 1992; Nio and Yang, 1991; Lafont, 1994; Davis and Dalrymple, 2011). The sandstones are deposited by lateral accretion in a meandering tide-controlled coastal system with mud drapes deposited by suspension fallout during slack water (Thomas et al., 1987). Megaripples and sigmoidal bedset indicate a stronger ebb tide influence than the reverse flood tide current ripples. This environment is interpreted as intertidal estuarine channel influenced by both fluvial and tide processes (Wheeler et al., 1990; Dalrymple et al., 1992).

Fluvial dominated delta front (FA8)

This FA shows sharp-based coarsening and thickening upward fine to coarse moderately sorted sandstones, highly bioturbated with *Ophiomorpha*, *Thalassinoides* and *Skolithos* ichnofacies (Fig. 6g). This facies association sequence varies from 2 to 10 m thick and contains dispersed gastropods, *Pectens* and oysters. According to the sedimentary fabric we can recognize two end-members (FA8.1 and 8.2). FA8.1 is characterized by common hydrodynamic bedding (trough cross bedding, tangential oblique or plane parallel bedding and compound cross stratifications). Some 5 to 10 cm thick claystone levels are observed on the bottom of the facies association and are missing upward. The 0.2 to 1.5 m thick bedset pattern varies from tabular (Fig. 6g) to steeply inclined (up to 25°; Fig. 6f). The FA8.2 facies association end-member presents thickening and coarsening upward fine to coarse sandstones with intercalations of 2 to 15 cm thick bluish gray silty claystone that define 0.2 to 1 m sandy bedset. Mud draped 5 to 10 cm thick sigmoidal cross-bedded coarse to medium grained sandstones are

observed along gentle slope progradation surfaces in a rhythmic 0.5 to 5 cm thick thin-thick bedding style, with reactivation surfaces and mud clasts lag deposits. Flaser bedding and reverse current are observed in fine grained facies.

The bioturbation and bioclasts recognized in both end-members suggest a strong marine influence. The sedimentary structures and plant debris described in AF8.1 end-member indicate the overall progradation of a delta front fed by hyperpycnal flows and bedload processes (Elliott, 1976, 1986; Bhattacharya and MacEachern, 2006; Olivero et al., 2008) and is described as a flood-dominated river-deltaic system by Mutti et al. (2000). The weak preservation of fine grained sediments indicates the influence of the fair weather wave in these prograding foreset. Compound cross stratification indicates bypass and turbulent flow processes followed by waning flow stage (Mutti et al., 2000). The thickening and coarsening upward FA8.2 sequence is interpreted as a fluvial dominated delta front and differs from the FA 8.1 by the strong tidal influence.

Subtidal bar (FA9)

This FA shows moderately sorted coarse to fine bioturbed sandstones including *Thalassinoides*, *Skolithos* and *Ophiomorpha* ichnofacies. The sedimentary fabric shows 1 to 20 cm thick bedsets separated by 0.5 to 1 cm thick mud couplets, and organized in a rhythmic thick/thin bed alternation with an overall sigmoidal cross-stratification pattern. Bedsets bases are tangential and their tops are commonly truncated by reactivation surfaces (Fig. 6i). Polymodal current directions are sometime observed. The basal surface is sharp, non-erosive (Fig. 6h) and locally shows ball-and-pillow load structures. Plant debris, bioclasts (mollusk shells, *Nummulitids* and *Alveolina*) and mudclasts are also observed. This facies association is about 1 to 5 m thick.

This FA is dominated by semi-diurnal tides (Dalrymple et al., 1992) and neap-spring-neap cycles (Mazumder and Arima, 2005). We interpret these deposits as subtidal bars affected by changes in flow velocity with reverse subordinate flow (Davis and Dalrymple, 2011).

Inner carbonate platform (FA10)

This FA is characterized *Miliolids*, *Alveolina* and *Orbitolites*, green algae, oysters and gasteropods bearing wackstones to grainstones (Fig. 6j). The FA presents nodular bedding with a sandy fraction. 20 to 50 cm thick marl intercalations occur sometime with *Lucina* bivalves in life position. The facies association thickness varies from 0.5 to 50 m.

This FA is interpreted as an inner carbonate platform (Geel, 2000; Brasier, 1975) slightly reworked by wave action. The marly intercalations indicate a quiet environment corresponding to a lagoon in a proximal inner carbonate platform (Hamon et al., 2016).

Prodelta deposits (FA11)

This FA consists of coarsening and thickening upward highly bioturbated massive poorly sorted grey muddy siltstone alternating with medium grained sandstones including shell fragments (echinoids, oysters) and whole specimens of *Nummulitids* and *Assilina* (Fig. 6k). Current ripples are observed in the fine grained facies. The muddy siltstone / sand ratio is always >1 . All of the beds display a tabular geometry into distances of more than 50 m. This 2 to 15 m thick facies association is burrowed by *Skolithos*, *Ophiomorpha* and *Thalassinoides*.

These deposits are interpreted as suspension settling from sediment-laded hyperpycnal flows of hemipelagic plumes (Orton and Reading, 1993) or pycnocline processes

created by internal waves (Mateu-Vicens et al., 2012) in a prodeltaic open marine environment below the fair-weather wave base level.

Turbiditic shelf environment (FA12)

This FA show heterolithic facies including silty marls and rippled medium to very fine grained 5 to 20 cm thick fining upward sandstones beds (Fig.6l). The base is sharp and slightly erosive with flute and groove marks and locally shows lag deposits, clay-chips and plant debris. Sandstone beds show a massive base passing upward to plane parallel laminations and to current ripples or combined wave-current ripples on top. Some hummocky cross-stratifications are locally visible. The top of sandstone passes gradually upward to nummulitids-bearing clayey facies. This 0.5 to 2 m thick FA is found together with prodelta deposits (FA11) and greyish marly offshore deposits (FA15).

This FA strongly suggests open marine shelf deposits submitted to rhythmic waning turbiditic flow discharges under unidirectional bedload processes, occasionally remobilized by wave action (Leckie and Walker, 1982; Brenchley et al., 1986; Mulder and Alexander, 2001; Dumas and Arnott, 2006; Girard et al., 2012;) below the fair-weather wave base. These deposits are recognized by many authors as hyperpycnites (Mulder et al., 2003; Mutti et al., 2000, 2003; Plink-Björklund and Steel, 2004; Petter and Steel, 2006; Olariu et al., 2010; Poyatos-Moré, 2014) generated by hydraulic jumps in front of the foresets of sediment-laden dense flow produced during extreme river flood events. These deposits shows reworking by oscillatory component giving low gradient topographic profile to this facies association deposited in upper offshore shelf environment with a water depth ranging from 35 m to 150 m (Postma and Drinia, 1993).

Reef environment (FA13)

This FA shows two main facies. The first facies (FA13.1) is a 2 to 8 m thick wackstone to boundstone dominated by perforated corals (*Actinacididae*, *Poritidae*, *Faviidae*; Leturcq, 1999), and encrusted by red algae (Fig. 6m-o). The surrounding matrix is a wackstone / packstone including *Solenomeris* fragments, *Alveolina* and *Orbitolites*. The proportion of *Solenomeris* increase towards the top of the construction, and coral reworked fragments can also be observed. The second facies (FA13.2) is a 5 to 20 m thick bindstone with *Solenomeris* encrusted by red algae (Fig. 6p). Occurrence of packstone matrix with *Nummulitids*, *Alveolina*, *Miliolids* and glauconite grains are observed. These facies are recognized as reworked deposits in a packstone / wackstone with *Nummulitids*, *Alveolina* and *Miliolid* matrix (FA13.3).

The coral dominated facies (FA13.1) occurs under mesophotic to oligotrophic conditions above fair weather wave base, either in high energy water depth probably less than 30 m, allowing the mixing of waters that reduces turbidity (Leinfelder, 2002; Morsilli et al., 2012; Hamon et al., 2016). This takes place in a distal inner carbonate platform setting. The bindstone with *Solenomeris* (FA13.2) indicate deeper water environments in mesotrophic conditions and suggest a proximal mid carbonate platform setting. The reworked facies (FA13.3) correspond to the dismantling part of the bioconstructions.

Mid carbonate platform (FA14)

This 2 to 15 m thick FA consists of a nodular wackstone to packstone (Fig. 6q) showing high concentrations of *Nummulitids* and *Operculine* founded together with *Alveolina*, *Miliolid*, *Orbitolites*, oysters, and echinoderms in variable proportions (Fig. 6r). Some intercalations of massive to hummocky cross-stratified 5 to 10 cm thick fine to medium

grained sandstone are observed. This facies association can be observed in the extensive outcrop (more than 500 m wide).

This FA juxtaposes shallow marine faunal assemblage (*Alveolina*, *Miliolids*, *Orbitolite*) with deeper faunal assemblage environment (*Nummulitids* and *Operculine*) suggesting transportation from a shallow to a more distal environment, probably by storm processes (Rasser et al., 2005). This is confirmed by the presence of hummocky cross stratification (upper offshore) that attests a mid-carbonate platform setting below fair weather wave base level.

Offshore environment and outer carbonate platform (FA15)

This FA is dominated by clayey facies containing *Nummulitids*. Locally 1 to 3 m thick interval are interbedded with medium to fine grained 10 to 20 cm thick plane-parallel laminated sandstone passing laterally to hummocky cross-stratified sandstone. The base is erosive with flute marks and pebbly lag deposits marked by aligned *Nummulitids*. Combined wave-current ripples can rework the top of the sequence. Skolithos, Planolites, Cruziana and Ophiomorpha ichnofacies were recognized. This clayey facies can also present some occurrences of (1) 0.2 to 1 m thick sigmoidal mud draped sandstones, and (2) 0.5 to 2 m thick massive and bioturbated bioclastic fine-grained sandy limestone with reworked shell debris (*Nummulitids*, *Pecten*, echinoderms).

This FA is interpreted as suspension fall-out in an upper offshore environment (30 to 60 m water depth) submitted occasionally to storm processes and distal tide influence below the fair-weather wave base (Dott and Bourgeois, 1982). Thick intervals ranging from 20 to 200 m thick of nummulitic clayey facies with the absence of hydrodynamic sedimentary structure and sandstone suggest very low energy conditions in lower

offshore environment (or outer carbonate platform) below the storm wave base with a 60 to 200 m water depth.

Slope environment (FA16)

This FA shows slumped laminated silty claystone and sandstone beds with a thickness of 1 to 50 m (Fig. 6u). Clayey matrix supported disorganized carbonate or sandstone 5 cm to 30 cm pebble to cobble thick in average are in mostly observed compared to clay-poor sandy matrix. In the Campo section, carbonate olistoliths show reworked fauna (*Alveolina*, *Nummulitids*, red algae, and corals). Between Lacort and Atiart sections, azoic clayey slumped facies unconformably seal successive slump scars in FA16 (Fig. 6v).

This FA shows syndimentary deformations and reworking structures (slumps and debris flows) originating from calcareous or siliciclastic shelf. This is consistent with slope-induced slumping and mass-flow transportation under gravity flows along an unstable shelf margin. The slumped facies and the clayey matrix supported debris flows indicate mainly cohesive flows.

Turbiditic basin (FA17)

This FA shows amalgamated tabular fining upward 0.2 to 10 m thick very coarse to medium grained sandstone beds with massive or plane-parallel laminations (Fig. 5w). The base is erosive with flute and groove casts and shows mudclasts, bioclastic pebble lag deposits and plant debris. The base of sandstones shows flame structure that inject substrate claystone and silt into the bed, corresponding to creep structure (with asymmetric flame) or load structures (with symmetric flame). Horizontal burrows of Paleodictyon and Helminthorhapse ichnofacies are observed. Laterally, this facies evolves to slightly amalgamated 10 to 20 cm thick plane-parallel to climbing rippled

fine to medium grained sandstones intercalated with brownish to dark silty-claystone organized in an overall fining and thinning upward sequence. Some mass transport deposits and slumps are locally observed.

This FA is interpreted as channelized high density turbiditic flows caused by high discharge in a deep water environment (Heard and Pickering, 2008) and associated with suspension fallout. The presence of climbing ripples implies suspension fallout combined with traction processes, typical of waning turbiditic flows (Walker, 1985). The heterolithic facies is interpreted as inter-channel deposits (crevasse splay or levees). Shelf faunal assemblage and plant debris reworked at the base of the sequence suggest sediment transportation through the shelf from the continental domain. The abundance of slump or debris flows attests to an unstable slope environment and possible canyon margin destabilization. This environment is interpreted as an amalgamated turbiditic channel complex.

4.1.2. Environmental partitioning and depositional systems

Four large-scale depositional systems corresponding to an assemblage of depositional environments were reconstructed (Fig. 7), and differ mostly by the dominant sedimentological processes involved, which mean that depositional environments and water depth evolution along the system can be reconstructed using modern analogs. This is further used to reconstitute the syn-sedimentary deposition profile using bathymetric estimations suggested in each depositional system.

Distally steepened mixed carbonate platform system

This system is dominated by carbonate environments (Fig. 7a). In the proximal parts of the platform, the dominant environment corresponds to inner platform *Alveolina*-rich carbonates (FA10; Figs. 5, 6j), with locally intercalated deltas (FA8.1; Fig. 5) deposited

into a restricted marine / lagoonal environment (Eichenseer and Luterbacher, 1992; Leturcq, 1999; Hamon et al., 2016). The inner platform *Alveolina*-rich limestones pass distally to more marly deposits (*Nummulitids*-rich wackestones) locally reworked by storms, in a mid-platform environment (FA14; Figs. 5, 6 q-t, 7a). The transition between inner and mid-platform is locally characterized by the presence of coral and red algae-rich reefal environments (FA13; Figs. 5, 6 m-p). The most distal part of this profile shows marly outer platform deposits with *Nummulitids* and *Assilina* (FA15; Figs. 5, 7a). Locally, in the Campo section (Fig. 3), the platform is oversteepened and slope deposits are observed with slumps, carbonate debris flows (FA16; Fig. 5) showing reworked *Alveolina*, *Nummulitids*, red algae and corals previously deposited in mid platform faunal assemblages, which indicate that the slope occurs in a mid-platform setting. This indicates the presence of a distally steepened ramp system (Fig. 7a), according to the classifications of Wright and Burchette (1998) and Pomar (2001). The bathymetric estimation ranges from 0-15 m water depth in the inner ramp (Tosquella, 1988), with lagoonal environments between 0-10 m water depth (Huyghe et al. 2012). The bathymetry in the mid-ramp is estimated between 15 to 60 m water depth and from 60 to 120 m water depth for the outer ramp, according to fauna living depth range (Geel, 2000). This system corresponds to the *Alveolina* Limestone, Riguala Marls and La Puebla Limestone Formations (Fig. 4).

Mixed tidal / deltaic platform system

The proximal part of the system consists of tide-influenced muddy environments (FA6; Fig. 5), locally intersected by river dominated deltaic systems with tide influence (FA 8.1; Figs. 6h, 7b) and associated prodelta deposits. The main depositional environments are interpreted as tidal flats to bays, which can laterally evolve into a shallow carbonate

platform, with environments ranging from inner to mid platform (FA10, FA14; Fig. 5). Some subtidal bars are recognized (FA9; Figs. 5, 6h). The distal part of the system corresponds to offshore silty marls (FA15; Fig. 5). We consider a maximum of 30 m water depth for the bay environments, and a range from 5 m to 20 m water depth for delta front with a maximum depth of around 50 m for the distal prodeltaic environment (Molenaar and Martinius, 1996). This mixed tidal / deltaic platform system corresponds to the middle Ypresian (lower Cuisian) deposits between the Roda de Isabena and Tremp areas (Roda Formation, Upper Detritic Complex, Suerri, Mur-Puigvert and Porredo deltaic systems) (Fonnesu, 1984; Yang and Nio, 1985, 1989; Eichenseer, 1988; Tosquella, 1988; Molenaar, 1990; Crumeyrolle et al., 1992; López-Blanco et al., 2003; Tinterri, 2007; Leren et al., 2010; Olariu et al., 2012) (Fig. 4).

Tide-dominated deltaic system

This system is dominantly clastic (Fig. 7c), with the proximal part showing alluvial fans (Hwang et al., 1995; Galloway and Hobday, 1996) (FA1; Figs. 5, 6a), passing downstream to braided stream, organized into sheet-like bodies, (FA 2.2; Fig. 5) and meandering channels (FA3; Figs. 5, 6c, 7c). The coastal domain is composed of river-dominated distributary channels (FA5; Figs. 5, 6d) in delta plain settings passing distally to an intertidal area with tidal channels (FA7; Figs. 5, 6e) and restricted brackish interdistributary bays (FA6; Figs. 5, 7c). Tidal processes are dominant on this system, and tide dominated deltas are well preserved (FA8.2; Figs. 6i, d, 7c). Distally, the system is gradually dominated by offshore shelf deposits (FA15, Fig. 7c), where the tidal effect is still present but more difficult to recognize. This depositional system is interpreted, in the littoral domain, as a tide-dominated delta (in the sense of Galloway, 1975; Wheeler et al., 1990; Dalrymple et al., 1992; Martinius, 2012). The Gange-

Brahmaputra delta (Michels et al., 1998) should correspond to a modern analog, and shows a tidal range of 4 m (macrotidal setting; Longhitano, 2008), a base of the delta front at 50 m water depth and the base of the prodelta at 75 m water depth. The brackish bay environment water depth is considered at 5 m (Martinius and Molenaar 1996). An alluvial fan continental slope should vary from 1° - 0.6° in proximal areas to 0.1° in distal parts (Boothroyd, 1972). An average slope for proximal sandy streams is 0.04° and 0.02° for meander streams and alluvial plain continental slope (Hickin and Nanson, 1984). This system is recognized in the Castigaleu and Montllobat Formations (Nijman and Nio, 1975; Van Der Meulen, 1983; Mutti et al., 1988; Nijman, 1998).

Distally steepened fluvial dominated deltaic system

The proximal part of this depositional system (Fig. 7d) shows a continental domain with a multistorey braided belt channels (FA 2.1; Figs. 5, 6b) organized in fluvial sheet-like channel bodies with high interconnectivity, passing distally to ribbon shaped channels (FA 2.3; Fig. 5). The low angle delta front environment is dominated by fluvial bedload transport (FA 8.1; Fig. 6g). More distally, the prodelta environment (FA11; Figs. 6k, 7d) is dominated by suspended load processes and diluted density flows with hypopycnal and hyperpycnal flow deposits (Orton and Reading, 1993; Mutti et al., 2000, 2003) with intercalation of shelfal turbidites (FA12; Figs. 5, 6l). This system evolves downstream into slope and basinal settings (FA16; Figs. 6u, 7d) with turbidite channels (FA17; Figs. 5, 6w) at the mouth of submarine canyons (e.g., Atiart surface; Figs. 4, 6v). The erosion and infill of turbidite channels are caused first by gravity-driven flows (Mulder and Alexander, 2001) or by fluvial hyperpycnal flows due to (1) slope gradient increase, or (2) high fluvial discharge with high sediment concentration (Mutti and Normark, 1987). The littoral domain is characterized by the dominance of

fluvial processes and corresponds to a river-dominated deltaic system with a distally steepened slope locally incised by a large-scale submarine canyon (Fig. 7d). This depositional system is characteristic of the Castissent Formation. The distal turbidite systems correspond to the Arro and Fosado channels (Mutti et al., 1988) (Fig. 4). Braided stream slope is from 0.08° to 0.06° (Hickin and Nanson, 1984). The Ebro delta modern analog shows a delta slope gradient of 0.0087 m/m^{-1} (Reading, 2009). With a length of the Castissent delta front close to 4 km, this gradient also suggests a water depth of 35 m for the delta front deposits. The deepest part of the turbiditic Ainsa Basin is in the range 400 to 800 m (Heard and Pickering, 2008). We focus on the proximal margin of the Ainsa-Basin showing a canyon and slope system with a bathymetric range from 150 to 200 m water depth, and a proximal part of the turbiditic basin from 200 to 400 m water depth.

4.2. Regional stratigraphic correlations

4.2.1. General profile reconstruction

In order to understand the sequential and longitudinal evolution of sedimentary environments within each proposed depositional system, we have juxtaposed these along idealized profiles (Fig. 7e). Each of the four depositional systems previously described were subdivided according to the position of several marine reference lines or key transition zones. The Bay Line corresponds to the transition between continental domain (fluvial channel and floodplain deposits) and the littoral domain (bay environment, deltaic plain or inner platform) and is well recognized in the four systems. The High Tide Sea Level is defining in the tide dominated deltaic system as the transition between the distributary channel and the bay environment with tide channel. The Low Tide Sea Level is recognize in the same system as the transition between the

intertidal domain (with bay and tide channel) and the subtidal area marked by the subtidal sandbar. The Fair Weather Wave Base is defined as the lower boundary of high hydrodynamic environments, i.e. the inner platform in the carbonate system, and the delta front in deltaic systems. The Storm Weather Wave Base is recognized where any evidence of storm deposits are found in the offshore or outer platform environments. The idealized profile reconstructed is subdivided in eleven areas that represent the same range of bathymetry. This general depositional chart shows a complete proximal-distal partitioning where all facies associations can be located. The vertical succession of the depositional environments along this general profile can be thus associated with shallowing or deepening trends and therefore allows for the determination of different stratigraphic sequences and their expressions in each section (Fig. 7f).

4.2.2. Estimated absolute age model and sequence hierarchy

With the aim to propose a sequence duration time-scale, we estimated an absolute age model based on previous published studies but updated to the Geological Time Scale 2012 (Hottinger, 1960; Hottinger and Schaub, 1960; Samsó et al., 1990; Tosquella et al., 1990, 1996; Serra-Kiel et al., 1994, 1998; Bentham and Burbank, 1996; Payros et al., 2009). These data show that some sequence boundaries or transgressive surfaces are closed to a limit of biozone or Chron (represented by green pins in Fig. 8), which allows us to propose age estimation:

- the first sequence boundary (SB1) corresponds to the Paleocene Eocene Thermal Maximum, and marks the limit between the Paleocene/Eocene (Pujalte et al., 2009b), dated to 56 Ma by Geological Time Scale 2012;
- the second transgressive surface (TS2) corresponds to the top of the Alveolina Limestone, dated close to the transition between SBZ5 and SBZ6 by Serra-Kiel et al. (1994) at 55.2 Ma from the Geological Time Scale 2012;

- the third sequence boundary (SB3) corresponds to the base of SBZ9 (Serra-Kiel et al., 1994) and is located in the reverse C24n.1r Chron. An age of 53.4 Ma is proposed;
- the fourth sequence boundary (SB4) is close to the transition between SBZ 9 and SBZ10 (Serra-Kiel et al., 1994), i.e., at 52.9 Ma;
- the fifth sequence boundary (SB5), i.e., the base of the Castigaleu Fm., belongs to SBZ10 and is dated close to the magnetic inversion between C23r and tC23n.2n (Bentham and Burbank, 1996), at 51.9 Ma;
- the sixth sequence boundary (SB6) may be recognized close to the limit between C23n.2n and C23.1r Chrons (Bentham and Burbank, 1996), at 51 Ma;
- the basal surface of the Castissent (seventh sequence boundary) is located at the base of SBZ11, and close to the transition between Chrons C23n.1n and C22r, i.e., at 50.6 Ma;
- the top of the Castissent Formation, i.e. the eighth transgressive surface (TS8), is recognized by a glauconitic level by Mochales et al. (2012) at the top of C22r, and an age of 49.6 Ma is proposed.

The vertical evolution of depositional environments (from A to K) shows three hierarchized sequence levels: Short Term, Long Term, and Depositional Sequences (Figs. 9-11). The first level is Short Term Sequences (STS) that delineate seventeen shallowing-deepening 10 m to 200 m thick cycles. Considering that the studied succession shows a duration of about 6.4 Ma, and if we assume that the seventeen Short Term Sequences have about the same duration, each of these Short Term Sequences would have a period of about 400,000 years that correspond to the 5th order of Vail et al. (1991) (Fig. 8). The Short Term Sequences are bounded by Maximum Flooding Surfaces, and correspond to genetic units (Galloway, 1989) or parasequences (Van Wagoner et al., 1988). The second and third levels defined here correspond to Depositional Sequences (Vail et al., 1977; Posamentier and Vail, 1988; Van Wagoner et al., 1988) or 3rd order of sequence from Vail et al. (1991) based on cycle duration and using subaerial unconformities (or their correlative surface; Mitchum, 1977) as sequence boundaries (Fig. 8). The eight Long Term Sequences (LTS) present an average duration of 800,000 years, are generally several hundreds of meters thick, and

are composed of several stacked Short Term Sequences (Fig. 8). The four Depositional sequences defined in this paper record 1-3 Ma/cycle and correspond to the lowest frequency cycles, by grouping several Long Term Sequences together (Fig. 8).

4.2.4. Regional correlation transect

The early Eocene Tresp-Graus-Ainsa basin succession is split into eight Long Term Sequences grouped in turn into four Depositional Sequences (TE) bounded by regionally mappable sequence boundaries (Fig. 12a).

Long Term Sequences A and B (TE1)

The base of Long Term Sequence A (LTS A) corresponds to a regional erosive surface on top of floodplain deposits in proximal parts of the basin (Figs. 9, 10) evolving basinward to a karstification surface on inner carbonate platform deposits (Campo section; Fig. 11) interpreted as the sequence boundary SB1. In the eastern part of the basin, this sequence boundary is overlain by alluvial fan conglomerate deposits passing distally to fluvial channels overlain by floodplain deposits (South Ribagorzana and Isabena sections; Figs. 9, 10) and inner carbonate platform alternating with greenish marls (Campo section; Fig. 11). These deposits are organized in an aggrading trend and are topped by a sharp transition between the reddish floodplain deposits and shallow marine carbonates. The latter are based by a conglomeratic and bioclastic lag deposit interpreted as the transgressive surface TS1. The overlying marine sequence evolves upwards to outer shelf deposits in an overall transgressive trend where the maximum flooding surface MFS1 is located.

The Long Term Sequence B shows an abrupt downward shift of depositional environments on the previous outer platform deposits interpreted as the sequence boundary SB2. It is characterized by the setting of (1) inner carbonate platform deposits

(Fig. 9), (2) clastic fluvial delta (Isabena section; Fig. 10), (3) reefal bioconstructions (Berganuy, Iscles Reef sections; Fig. 12), and (4) slope deposits with olistoliths and some turbiditic events (Campo section; Fig. 11). These sequences form an aggrading trend bounded by the transgressive surface TS2 that marks a thick interval of outer carbonate platform deposits (Fig. 12) topped by the maximum flooding surface MFS2. The Long Term Sequences A and B are characterized by the dominance of a distally steepened mixed carbonate platform system (Fig. 7a) with very local clastic input sourced from a northern area (Hamon et al., 2016). They are grouped in the Depositional Sequence TE1 showing an aggrading trend from SB1 to TS2 and a transgressive trend from the TS2 to the MFS2.

Long Term Sequences C and D (TE2)

The Long Term Sequence C starts with an abrupt downward shift of the depositional environment interpreted as the sequence boundary SB3. It is marked by a mixed tidal/deltaic platform system that overlaps previous outer platform deposits (South Ribagorzana to Isabena sections; Figs. 9, 10, 12). In the Campo section, the SB3 is placed at the base of a decameter-thick complex of olistoliths (Fig. 11) and it is pinned at the base of shelfal turbidites that seal marly outer platform deposits in the Atiart section (Fig. 11). These deposits form an overall aggrading trend ending with the transgressive surface TS3 that marks the deepening of the depositional system with bay deposits that pass distally to offshore and slope environments (Fig. 12). In the South Ribagorzana section, this system shows inner carbonate platform passing distally to a mid and outer carbonate platform deposits (Fig. 9).

The Long Term Sequence D is characterized by an abrupt downward shift of the depositional environments (sequence boundary SB4) with distributary channel and

deltaic environments overlying (1) shallow marine environment (between Berganuy and Iscles Reef sections; Fig. 12), and (2) offshore deposits (Isabena and Montanana section; Figs. 10, 12). More distally, in the Campo section SB4 is pinned at the base of a slumped package of outer shelf marls and it is placed at the base of shelfal turbidite deposits in the Atiart section (Fig. 11). The Long Term Sequence D forms an overall aggrading interval bounded by the transgressive surface TS4 marked by the deepening of the depositional environments with the setting of offshore deposits (Fig. 12). The Long Term Sequences C and D correspond to a high clastic supply with the development of several deltaic systems sourced from the north and influenced by tidal processes (e.g., Roda Sandstone and Suerri System; Fomesu, 1984; Crumeyrolle et al., 1992; López-Blanco et al., 2003; Tinterri, 2007; Leren et al., 2010; Olariu et al., 2012) (Fig. 7b). These two Long Term Sequences are grouped into the TE2 Depositional Sequence with an aggrading trend defined from the SB3 to the TS4 followed by a transgressive trend up to MFS4.

Long Term Sequences E and F (TE3)

The base of Long Term Sequence E is marked by a sharp and erosive downward shift of the depositional environments, interpreted as the sequence boundary SB5. This sequence shows intermediate sheet-like fluvial bodies in the proximal part in the South Ribagorzana and Tremp sections (Fig. 9), passing downstream to (1) amalgamated distributary channels in the Isabena section (Fig. 10), (2) tide dominated delta fronts in the Campo section (Fig. 11), and (3) prodelta and offshore deposits associated with shelfal turbiditic in the Lacort and Atiart sections (Fig. 11). The succession is organized in a transgressive trend marked in the continental domain by an evolution from braided to meandering channels (Fig. 9) and some marine influences on top of fluvial channels.

In the littoral domain, the transgressive trend shows an increase of marine influence marked by tidal channel intercalations passing to thick bay deposits (Fig. 10). In the distal part of the basin, tide dominated distal mouth bars evolve to offshore deposits with less storms reworking (Fig. 11). The topmost part of this trend corresponds to the maximum flooding surface MFS5.

The base of the Long Term Sequence F shows an abrupt downward shift of depositional environments interpreted as sequence boundary SB6. It is characterized by a conglomeratic alluvial stream flow fan in the eastern part of the Graus-Tremp Basin (Figs. 9, 12) passing distally in the Isabena section to a stack of distributary channels with abundant coal debris (Fig. 10) and to a prograding tide-dominated delta front in the Campo section (Fig. 11). These deposits form a transgressive trend evidenced by (1) an increase of floodplain deposits in continental domain (Fig. 9), (2) a thick interval of bay deposits with important oyster's accumulation in the littoral domain (Fig. 10), and by (3) a noticeable *Nummulitids*-rich carbonate bed in the offshore environments of the Campo section (Fig. 11). The latter is interpreted as the maximum flooding surface MFS6.

These two Long Term Sequences are grouped together in the TE3 Depositional Sequence which shows a significant turnaround in sedimentation style with the clear dominance of clastic input and the development of a large tide-influenced fluvio-deltaic system, prograding to the west (Fig. 7c). TE3 corresponds to a major transgressive trend bounded by SB5 and MFS6.

Long Term Sequences G and H (TE4)

The base of the Long Term Sequence G corresponds to a regional erosional surface that marks an abrupt downward shift of depositional environment interpreted as sequence

boundary SB7. This sequence shows a continuous multistorey braided channel belt in the proximal part of the Graus-Tremp Basin (Fig. 9), passing distally to fluvial dominated delta fronts with some tidal influences in the Campo section (Fig. 11). In the eastern part of the Ainsa Basin, SB7 is correlated with the erosive surface of the Atiart submarine incision, and is overlain by slope deposits with low-density turbidites (Figs. 11, 12). These deposits are organized in an aggrading trend topped by the transgressive surface TS7. The latter is evidenced by (1) the appearance of a major paleosol on top of multistorey braided channel belt (Fig. 9), (2) an extensive conglomeratic lag deposit eroding the fluvial channel sequence (Fig. 10), (3) a *Nummulitids*-rich interval directly overlaying a distributary channel (Fig. 11), and (4) a maximum of amalgamation of turbiditic channels in the Fosado turbiditic channels complex that passes to slope deposits with fewer turbiditic events (Figs. 11, 12). This succession is followed by an overall deepening upwards trend including floodplain to coastal plain deposits in the proximal part of the basin (Fig. 9), passing distally to *Nummulitids*-rich offshore deposits in the Campo section (Fig. 11), and finally to slope and basinal shales in the distal setting of Atiart section (Fig. 11). It is capped by the maximum flooding surface MFS7.

The Long Term Sequence H is pinned by an abrupt downward shift of the depositional environment reported to sequence boundary SB8. From east to west, this sequence is characterized upstream by a multistorey braided channel belts (South Ribagorzana and Montanana section; Fig. 9), passing to ribbon braided channels (Isabena section; Fig. 10), distributary channels and fluvial-dominated delta front systems without tidal influence (Campo section; Fig. 11), and to prodelta and slope deposits downstream. These deposits show an aggrading trend, ended by paleosols on top of amalgamated

fluvial channels (Fig. 9) that are interpreted as transgressive surface TS8. This transgressive surface corresponds laterally to a thin oyster bed on top of a fluvial channel (Isabena section; Fig. 10) and the maximum stage of deltaic progradation in the littoral setting. This transgressive trend is topped by the maximum flooding surface MFS8 well identified in the Isabena section by oyster accumulations in a bay environment (Fig. 10) and by an *Assilina*-rich wackestone in the Atiart section (Fig. 11). The Long Term Sequences G and H correspond to a thin, highly regressive and amalgamated fluvial-dominated system, passing abruptly from delta to basinal turbidite deposits (Fig. 7d) in a westward sediment routing. They are grouped in the TE4 Depositional Sequence which is bounded by SB7 and shows an aggrading trend up to TS8 and a transgressive trend up to MFS8.

5. Discussion

5.1. Recognition of a piggyback tectonic signal

One aim to isolate the control exerted specifically by piggyback tectonics from other regional controls (eustatic, climatic), is to distinguish the impacted spatial and time scales (local and regional scales; Fig. 1). The stratigraphic response at a regional scale (Fig. 1) is controlled by (1) eustasy, foreland flexural subsidence and isostatic rebound, which drive the regional creation of accommodation, and (2) climate and Pyrenees hinterland uplift, which control sediment supply. The local scale corresponds to the piggyback basin itself and is mainly controlled by intrabasinal tectonic structures (i.e., major thrust front ramps, trailing fault-bends, or fault-propagation folds growing above major ramps; Ori and Friend, 1984). The latter affect development of local accommodation by (1) decreasing the available space during uplift phases, and (2) controlling the intrabasinal compartmentalization and trapping of sediments in local

depocentres (Talling et al., 1995) (Fig. 1). Sediment supply can be modulated at this local scale by the uplift of basin margins and the emergence of local sediments sources by thrust propagation.

The regional external controlling factors will be equally recorded in all the sections, whereas the intrabasinal piggyback tectonic record will have a locally expression in the basin. Thus, we can recognize the intrabasinal piggyback tectonic impact by abrupt changes in sediment thickness and associated depositional stratigraphic geometry, depositional environment (i.e., major changes in stacking pattern), sedimentary process or changes in current directions and with local sedimentary unconformities.

In order to better evidence the influence of intrabasinal piggyback tectonics in the sedimentary record, we provide a palinspastic reconstruction of the successive Depositional Sequences into four paleogeographic maps (Fig. 13). We have reconstructed the maps before the Lutetian-Bartonian rotation events (Muñoz et al., 2013), removing the effect of the clockwise rotations events by an anticlockwise rotation of 60° in the western part to 30° in the Campo area, 15° in Isabena section area and 10° more eastward (according to Bentham and Burbank, 1996). The thrust displacement since the Lutetian is considered by applying a general translation of 71.5 km in the $N10^\circ$ direction. During the Ypresian, a total of a 9 km displacement is assumed for the Montsec Trust (Vergès, 1993). The restored paleocurrent data after rotation are given in Appendix B. The tectonic evolution through time is integrated for each paleogeographic maps (Fig. 13e). Facies partitioning and thickness variations are also studied through correlation transects restored to their syn-depositional position, with local tectonic structures indicated (Fig. 14).

5.2. Piggyback intrabasinal tectonic evidences in the early Eocene Tremp-Graus-Ainsa Basin

Four main periods during the early Eocene are recognized according to major changes in basin fill evolution.

Underfilled carbonate basin stage (TE1)

At the base of TE1, the alluvial conglomerate unit (Claret Conglomerate, Table 1) passes laterally southward to a thinner fluvial environment, close to the present-day Montsec thrust front (Figs. 13a, 14a). This suggests the growth of the Montsec as a blind thrust anticline as argued by Rosell et al. (2001). The following succession records local shallower conditions along the northern Tremp-Graus sub-basin margin allowing the development of reefs (e.g., Berganuy, Iscles, and Merli reefs) (Figs. 13a, 14a) on topographic highs that limit local depocentre as demonstrated by the thickness increase of nummulitic marls (FA15) in the Isabena, Iscles, Sola and Montañana sections (Figs. 12b, 14a). Rare clastic deltas, fed from the north, are trapped in these local depressions as along the Isabena section (Gaemers, 1978; Eichenseer and Luterbacher, 1992; Hamon et al., 2016) (Fig 13a). The Berganuy and Iscles reefs are aligned with the prolongation of the Coll Del Vent anticline, whereas the Merli reef developed on top of the Turbón anticline (Eichenseer, 1988; Vincent and Elliott, 1997) (Figs. 13a, 14a). The activity of the Turbón and Coll del Vent Anticlines is interpreted as Lower Cretaceous N-S transtensional structures, passively inverted during the southward displacement of the piggyback basin over the Montsec thrust (Vincent, 2001; López-Blanco et al., 2003). Montsec thrust activity is also recorded by the N-S evolution of the depositional environments between the Montañana, Tremp and South Ribagorzana sections in the eastern part of the basin (Fig. 13a), where the succession passes laterally from marly

outer platform deposits (FA15) in the basin depocentre to inner carbonate platform deposits (FA10) in the southern margin of the basin (Fig. 14a). This southward facies evolution is accompanied by a thickness decrease towards the Montsec high that indicated growth of the Montsec thrust. The lack of detrital sedimentation in the southern margin of the basin suggests that the Montsec high is a blind thrust anticline growing in submarine conditions (Fig. 12). This stage ends with the deposition of a homogeneous mid carbonate platform level (La Puebla Limestone Fm.) which shows no remarkable thickness and facies variations through the basin, including the Montsec area. This may suggest that this level is mainly due to a regional control. Baceta et al. (2011) describes an onlap of La Puebla Limestone Fm. on the underlying units near the Montsec high. This suggests that the underlying succession was already tilted by the propagation of the Montsec blind thrust before deposition of this limestone level. This indicates that the activity of the Montsec thrust ceased (at least temporally) at the end of TE1 and marks the end of a first major tectonically active period during which regional control factors are expressed.

Local clastic input in underfilled basin (TE2)

In the depocentre of the Tremp-Graus sub-basin (Montaña section, Figs. 9, 12, 13b), the base of TE2 shows outer platform deposits passing to inner platform carbonates near the Montsec area (South Ribagorçana section, Figs. 13b, 14b). Here, the lack of clastic sedimentation suggests a subaqueous position of the Montsec high between the Tremp-Graus and the Ager sub-basins, consistent with previous works (Mutti et al., 1988; Martinius, 2012). Unfortunately, this sequence is completely eroded close to the Montsec high by the later TE3 sequence boundary (SB5; Figs. 9, 12a). This differential erosion suggests an increase of uplift rate in the southern part of the Tremp-Graus sub-

basin, probably related to the growing of the Montsec structure. The Tremp-Graus sub-basin shows syncline geometry, marked by tide influenced deltaic systems fed from the north (from east to west: Porredo/Mur-Puigvert, Suerri, Montañana depocentre and Roda/UDC systems; Table 1, Fig. 13b). As in TE1, the northern margin of the Tremp-Graus sub-basin is affected by local tectonic movements during TE2, registered by local depocentre partitioning (Fig. 14b). In particular, the Coll del Vent anticline cause change in deltaic current direction with setting of deltas that prograde (1) toward the southeast in the eastern flank of the anticline and, (2) toward the southwest in the western flank (Fig 13b). This stage is also marked by the uplift of the Coll del Vent and Roda Fold anticlines that caused the confinement of the deltaic deposits (Roda Sandstones and Upper Detritic Complex delta; Crumeyrolle et al., 1992; Lopez-Blanco et al., 2003) in a depocentre which was subsequently filled (Leren et al., 2010). The Roda Fold System is interpreted as a fault-bend or oblique fold detachment related to the southward displacement of the Montsec thrust (López-Blanco et al., 2003). Westwards, in the Campo area (Fig. 3), TE2 shows outer shelf to slope deposits with olistoliths from a remobilized carbonate platform with coral debris (Figs. 12b, 13b, 14b). This indicates erosion of preexisting Merli reef buildups that was probably uplifted in the northern part by the Roda Fold System inducing a westward increase in slope gradient, consistent with slump destabilization towards the Campo section. As in the previous stage, the upper part of TE2 is characterized by progradation of another homogeneous mid carbonate platform level (the Morillo Limestone) in the western part of the basin (between Isabena and Atiart sections, Fig. 12b), suggesting a new intrabasinal tectonic quiescence period, which marks the end of the TE2 second tectonically active phase.

Overfilled stage and Montsec thrust emergence (TE3)

In the eastern part of the Tremp-Graus sub-basin, the erosion of the sequence boundary (SB5) at the base of TE3 increases towards the Montsec area (South Ribagorzana section; Figs. 9, 12, 14c). This SB5 erosive surface was previously described as an angular unconformity (Mutti et al., 1988; Nijman, 1998). To the west, erosion of SB5 is less important and corresponds, from the Campo to the Atiart section, to an abrupt basinward shift from marly outer shelf deposits to tide-dominated delta and shelf turbidites (Figs. 11, 12b, 14c). We interpret this surface as a peneplanation surface related to overall uplift of the basin, suggested in the Tremp-Graus sub-basin by the subaerial exposure and erosion of the Montsec blind thrust fold (Fig. 13c). This hypothesis is further supported by a change of mineralogical content of sandstones across the SB5 surface described in previous works. The arkosic sandstones of the underlying TE2 is interpreted as deriving from erosion of a local granite pluton cooled at 308 Ma (Molenaar and Martinius, 1990; López-Blanco et al., 2003; Whitchurch et al., 2011) whereas the litharenite composition of TE3 would evidence the establishment of new sediment sources by the cannibalization of previous Mesozoic or Cenozoic deposits (Nijman, 1998). Both this change of mineralogy and the peneplanation surface at SB5 imply the exhumation of new sediment sources supported by paleocurrent directions analysis that indicate north, east and southeast sources possibly linked to (1) increased emergence of the Montsec anticline, (2) uplift of the hanging wall section of the Segre Fault, which corresponds to the eastern lateral ramp of the Montsec thrust (Burbank et al., 1992), or (3) Bóixols thrust sheet emergence associated with the Tremp-Graus sub-basin uplift (Figs. 12b, 13c). This led to a reorganization of the sediment drainage

network with sources coming from the Axial Zone from an orogen-transverse drainage system (TE1 and TE2) to an orogen-parallel drainage system (TE3).

Piggy-back displacement and development of lateral ramps (TE4)

In the Tremp-Graus sub-basin, the TE4 depositional system changes drastically by the amalgamation of fluvial channels, which reflects a major decrease in accommodation space and overall higher energy conditions (Huerta et al., 2011). Moreover, the absence of clear tidal dominated deposits in the littoral domain is consistent with an increase of fluvial input on the shelf. These changes in depositional profile in addition to the significant decrease of sediment thickness during TE4 compared to TE3 suggest an overall decrease of accommodation/sediment supply ratio in the Tremp-Graus sub-basin during this period. However, in the Ainsa basin the TE4 sequence shows an opposite trend, with an overall deepening of the depositional system associated with an abrupt increase in sediment thickness (Figs. 12b, 14d) interpreted as an increase of accommodation /sediment supply ratio. The sequence boundary of TE4 (SB7) shows differentiation between the Tremp-Graus and the Ainsa sub-basin. To the east of the Foradada fault (Tremp-Graus sub-basin, Figs. 3 13d), the sequence boundary separates offshore deposits (TE3) from deltaic deposits (TE4) and indicates an overall basinward shift of the depositional systems that would be consistent with relative sea-level fall. By contrast, to the west of the fault (Ainsa sub-basin), the sequence boundary is expressed by a large submarine unconformity (Atiart surface), with a thick succession of slope deposits overlying and deeply incising distal offshore deposits (Long Term Sequence F; Figs. 12b, 14d). This change to a deepening-upward trend might result from abrupt relative sea-level rise. We interpret the decrease of the accommodation/sediment supply ratio in the Tremp-Graus sub-basin as a response of uplift associated with the Montsec

Thrust that caused a decrease in accommodation and a strong progradation of the fluvio-deltaic system, which is then forced to migrate westward, parallel to the Pyrenean range, and feeding the adjacent Ainsa sub-basin (Clevis et al., 2004) (Figs. 13d, 14d). Syn-sedimentary activity of the Montsec thrust during this period has been evidenced in several studies (e.g., Soler and Garrido, 1970; Nijman and Nio, 1975; Farrell et al., 1987; Muñoz et al., 1994; Nijman, 1998; Teixell and Muñoz, 2000). The opposite tendency between the Tremp-Graus and the Ainsa sub-basins could be also explained by differential intrabasinal tectonic activity expressed in two domains showing slope instabilities and abrupt changes in sediment thickness and depositional environments. The first of these domains is observed close to the Foradada fault, where the Long Term Sequence G comprises a 50 m-thick fluvial dominated deltaic system (Santo-Cristo Section, Figs. 12a, 14d), passing abruptly on the western side of the fault to a 400 m-thick series of slumped marly slope deposits (Lacort section; Figs. 12a, 14d). The western part of the Foradada fault is also marked by development of the Atiart submarine surface, with a series of slump scars that affect the underlying TE3. Farther westward, the Long Term Sequence G sequence shows a second major change, with 600 m-thick slope deposits passing to a more than 800 m-thick succession of marly slope deposits containing the Fosado turbidite channel complex (Mutti et al., 1988; Poyatos-Moré et al., 2014) (Fig. 14d). This second variation in thickness and depositional environments occurs abruptly along a relatively short distance (1.2 km, between Atiart and Pocino sections, Fig. 14d), across the Atiart thrust (Figs. 13d, 14d). We interpret these changes as the result of westward syn-sedimentary propagation of the Montsec thrust. The Atiart thrust would act as a Montsec Thrust lateral ramp structure (Fig. 14d), controlling the relative uplift of highly amalgamated fluvio-deltaic

systems in the continental domain (east), and the development of slope instabilities and turbidite systems in a highly subsiding and deep marine domain (west). This stage is therefore marked by differential evolution of the Tremp-Graus sub-basin which is integrated in the wedge-top depozone whereas the Ainsa sub-basin remains in the foredeep depozone. Furthermore, Atiart thrust development occurring at the wedge-top-foredeep transition is coupled with the activity of the Foradada tear-fault, accommodating southward displacement of the uplifted Tremp-Graus sub-basin from the relative immobile and subsiding Ainsa sub-basin (Séguret, 1972). During the Long Term Sequence H, any abrupt changes in sediment thickness and depositional environments are reported from either side of the Foradada tear-fault, suggesting a stop of the Foradada Fault activity at the end of TE4. The Atiart thrust impact on sedimentation is well recognized during Long Term Sequence H where prodeltaic progradation shows some incisions (Fig. 12 a, b). The first one, between the Atiart and Pocino sections, is covered and overlapped by the Arro turbidite system, westward in the San Esteban section. The second one is less well expressed and only recognized in the Pocino section (Fig. 12a). This surface could record the latest major pulse of the Atiart thrust (Muñoz et al., 2013). Furthermore, in the Pocino section, no major changes of depositional environment and sediment thickness have been observed in the overlying deposits (STS 17, Figs. 12b, 14d), which could provide a reference for the end of the Atiart thrust activity.

5.3. Towards a model of piggyback basin infill and associated stratigraphic signals

During the early Eocene, the Tremp-Graus-Ainsa Basin shows a complete piggyback evolution with four major tectonically-induced stages specific to piggyback basin

development (Fig. 14). This stage evolution corresponds to the emplacement of a single piggyback basin located in the hanging wall of one main frontal thrust, without any other thrust development that could induce emergence of new secondary sources or modulate the subsidence of the studied piggyback basin. The evolution of the Tremp-Graus-Ainsa Basin is interpreted as the result of the combination of different controlling factors that are intrinsic to a piggyback basin such as (1) piggyback uplift caused by the frontal thrust activity and controlling emergence of new sediments sources, and (2) orogenic uplift that controls regional flexural subsidence and sediment supply (Fig. 1). With the aim to provide a simplified piggyback basin infill model, our case study comparison only considers a piggyback basin (1) resulting from changes of these factors intrinsic to the piggyback basin evolution, and (2) located in the hangingwall of the frontal thrust (Evans and Elliott, 1999; Martín-Martín and Martín-Algarra, 2002; Gugliotta and Morticelli, 2012) (Fig. 15a, b). The upper part of the Scillato Basin (Gugliotta and Gasparo Morticelli, 2012), which results from another thrust sheet that increases sediment supply is not integrated in our model.

The first proposed stage of the piggyback basin infill corresponds to a thick retrogradational succession (Fig. 15d). This is well expressed in the Tremp-Graus sub-basin from the Claret Conglomerate to the Riguala offshore marls (TE1; Fig. 15c). The same succession is reported in the Barrême Basin (from the Poudingues d'Argens to the Marnes Bleues from Evans and Elliott, 1999) (Fig. 15b), and in the Scillato Basin (TS1 and TS2 from Gugliotta and Morticelli, 2012) (Fig. 15c). This retrogradational trend reflects a progressively higher accommodation/sediment supply ratio with the piggyback basin uplift not great enough to counterbalance regional flexural subsidence

(Fig. 15d). The relatively low clastic sediment supply that characterizes this underfilled stage is coming from the Axial Zone and could be linked to a low uplift rate of this area. The second stage shows an overall aggradational succession, but the basin remains underfilled (Fig. 15d). This stage correspond to the TE2 depositional Sequence in the Tremp-Graus sub-basin (Fig. 15c) and is equivalent to the succession from the Conglomérat de Clumant to the Conglomérat de St Lions in the Barrême Basin (Fig. 15b) and to the upper part of the TS2 sequence in the Scillato Basin (Fig. 15a). This trend shows an increase in clastic supply coming from the Axial Zone (Fig. 15d), recognized both by paleocurrent measurements and sediment provenance data in the Tremp-Graus and Barrême Basins (Molenaar and Martinius, 1990; Nijman, 1998; Evans and Elliott, 1999; López-Blanco et al., 2003; Whitchurch et al., 2011). The flexural subsidence remains quite high and strongly compensates the piggyback basin uplift and the increase in sediment supply (Fig. 15d). These two first stages are largely characterized by marine conditions and by sediments sourced from the Axial Zone, as is also described in the lower part of the Oligo-Aquitania succession of the Mula–Pliego Basin (Martín-Martín and Martín-Algarra, 2002).

The third stage corresponds to an overfilled stage with an aggrading / slightly retrograding succession, recognized in the TE3 Sequence of the Tremp-Graus sub-basin and in the Molasse Rouge Fm. to the Séries Grises Fm. of the Barrême Basin (Fig. 15b, c). This trend is induced by a major increase in sediment supply, helped by the emergence and erosion of sedimentary thrust sheets within the piggyback, providing new sediment sources (Fig. 15d). However, the accommodation remains high and is not compensated by piggyback basin uplift. The mineralogy and current direction in the Tremp-Graus Basin indicate northern sediment provenance coming from the Axial Zone

during TE1 and TE2, whereas TE3 shows sediment provenance from sedimentary thrust sheet. The Barrême basin succession also shows changes in sediment mineralogy and current direction passing from NE Alpine massifs provenance to SE Cretaceous provenance. This stage also records reorganization of the sedimentary drainage network passing from a dominantly orogen-transverse system, to an orogen-parallel drainage system. In the Scillato Basin, this stage is not recognized because of the emplacement of a new thrust sheet unit that induced a higher sediment supply, counterbalancing accommodation space creation and basin infill (Gugliotta and Gasparo Morticelli, 2012) (Fig. 15a). The final stage of piggyback basin development is marked by low accommodation aggrading succession corresponding to the TE4 Sequence in the Tremp-Graus sub-basin and to the Grès Vert Fm. in the Barrême Basin (Fig. 15b, c). Flexural subsidence in this stage is counterbalanced by piggyback basin uplift, induced by translation of the frontal thrust (Fig. 15d). This movement is marked by the development of lateral ramp structures, which separate the uplifted piggyback depocentre from an adjacent subsiding foredeep depocentre, where instabilities and turbidite systems can develop. This stage is characterized by an open piggyback basin according to the Suriano et al. (2015) classification, with an aggrading stage located above a main incision surface. During stages 3 and 4, sediments are mainly sourced from the sediment thrust sheet and erosion of the Axial Zone, as is also recognized in the Aquitanian upper part of the Mula–Pliego Basin succession (Martín-Martín and Martín-Algarra, 2002). In the Tremp-Graus-Ainsa Basin, this stage is the first one that leads to differentiation between the Graus-Tremp and the Ainsa sub-basins; the first one is include in the wedge-top depozone whereas the second one remains in the foredeep depozone.

The whole piggyback succession described in the Graus-Tremp-Ainsa Basin is stratigraphically marked by the development of major subaerial unconformities, followed by retrogradational or aggradational depositional trends. The basin infill therefore shows an absence of clear prograding trends. This would result from the recurrence of frontal thrust tectonic pulses that uplift the basin and cause formation of major subaerial unconformities at the piggyback basin scale. This activity is rapidly followed by aggrading or retrograding trends which record higher regional flexural accommodation space creation than sediment supply, except during the latest period of basin uplift (stage 4) where the sediment depocentre shifts to be in the foredeep domain.

6. Conclusions

The stratigraphic architecture of a piggyback basin infill is complex because of the recurrent interactions between orogenic dynamics (regional flexural subsidence, local piggyback-related structures), climate, and global eustasy, which largely control the balance between erosion and sedimentation. In this work, we propose to isolate the impact of intrabasinal tectonic control specific to piggyback basin development in the Tremp-Graus-Ainsa Basin during the early Eocene, with the aim to propose a first reference stratigraphic succession and provide a piggyback basin evolution model. The sedimentological and stratigraphic analysis performed at the basin scale evidence a three-fold depositional sequence hierarchy, in which the local intrabasinal tectonics is mainly expressed at the Long Term Sequence scale. The key result is the discrimination of four main stages specific to piggyback basin development, and which result from the combination of intrabasinal tectonic activity, regional flexural subsidence and Axial Zone uplift. The first stage shows a domination of Axial Zone dynamics with a very low sediment supply and high accommodation space resulting from low orogenic uplift and

high flexural subsidence, leading to an underfilled stage. The second stage remains still largely controlled by the Axial Zone with high flexural subsidence and an increase in clastic sediment supply coming from the growing Axial Zone. The frontal thrust propagation is expressed by a subaqueous high interpreted as a blind thrust fold in these two first stages. The third stage results from the emergence of sedimentary thrust sheets and the blind frontal thrust fold due to active intrabasinal tectonics. Sediments here are sourced both from the Axial Zone and the emerged thrust sheets and induce a drastic increase of sediment supply leading to the establishment of a drainage direction mainly parallel to the orogeny, and reflecting the beginning of the overfilled stage. The last stage corresponds to the main frontal thrust propagation movement, which strongly uplifts the basin and leads to the development of lateral ramp structures. This stage is mainly controlled by intrabasinal tectonics, which induce an overall decrease of the accommodation/sediment supply ratio and is marked by the development of a subsiding depocentre in the foredeep area.

The proposed model can provide some keys to unravel controlling factors in piggyback basin development, and help to identify the results of piggyback dynamics from other forcing factors. This reference stratigraphic succession corresponds to a single piggyback basin development emplaced during one main frontal thrust propagation. This simple case can be modulated by other regional controlling factors such as climate, orogen-scale tectonic events, or local tectonic events such as the setting of a new thrust sheet.

Acknowledgements

This study was funded by a PhD grant to Emmanuelle Chanvry from TOTAL SA, IFP Energies nouvelles and St Etienne School of Mines. TOTAL SA is thanked for its

financial support which has enabled several fieldworks. We would like to thank the Chief Editor J. Knight and the 2 reviewers for their helpful comments. Thanks to Etienne Fayolle, Nicolas Saspituri, Jean-Loup Rubino and Jean-Noël Ferry for their passionate discussions in the field. Many thanks are due to Youri Hamon, Quentin Daviau and Julien Schmitz for the participation to the realization of some sections. Many thanks to Michel Lopez for valuable discussion that improved the orientation of this article.

Appendices

Appendix A

The Appendix A is intended to provide detailed information of each section measured with location, section name and abbreviation, the GPS coordinates, the thickness, and the concerned Formations studied

Appendix B

The Appendix B shows initial paleocurrent data measured on the field and restored after the clockwise rotation event removing (Muñoz et al., 2013). The data are presented for each Long Term Sequence.

References

- Allen, J.R.L., 1963. Structure of ripple marks. *Nature* 198, 847–849.
- Allen, J.R.L., 1965. A review of the origin and characteristics of recent alluvial sediments. *Sedimentology* 5, 89–191.
- Allen, J.R.L., 1983. Studies in fluvial sedimentation: bars, bar-complexes and sandstone sheets (low-sinuosity braided streams) in the Brownstones (L. Devonian), Welsh Borders. *Sedimentary Geology* 33, 237–293.

Anadón, P., Cabrera, L., Colombo, F., Marzo, M., Riba, O., 1986. Syntectonic intraformational unconformities in alluvial fan deposits, eastern Ebro Basin margins (NE Spain). *Foreland Basins* 8, 259–271.

Anastasio, D.J., Mitra, S., Fisher, G.W. 1992. Structural evolution of the external Sierra, southern Pyrenees, Spain. In: Mitra, S., Fisher, G.W. (Eds.), *Structural Geology of Fold and Thrust Belts*. John Hopkins University Press, Baltimore, MD, pp. 239-251.

Ardèvol, L., Klimowitz, J., Malagón, J., Nagtegaal, P.J., 2000. Depositional sequence response to foreland deformation in the Upper Cretaceous of the Southern Pyrenees, Spain. *American Association of Petroleum Geologists Bulletin* 84, 566–587.

Baby, P., Moretti, I., Guillier, B., Limachi, R., Mendez, E., Oller, J., Specht, M., 1995. Petroleum system of the northern and central Bolivian sub-Andean zone. In: Tankard, A.J., Suárez, R.S., Welsink, H.J. (Eds.), *Petroleum basins of South America*, Memoir. American Association of Petroleum Geologists vol. 62pp. 445–458.

Baceta, J.I., Pujalte, V., Wright, V.P., Schmitz, B., 2011. Carbonate platform models, sea-level changes and extreme climatic events during the Paleocene-early Eocene greenhouse interval: a basin-platform-coastal plain transect across the southern Pyrenean basin. In: Arenas, C., Pomar, L., Colombo, F. (Eds.), *Pre-Meeting Field-Trips Guidebook*. Zaragoza, 28th IAS Meeting, Geo-Guías, 7, Sociedad Geológica de España, Zaragoza, pp. 101–150.

Baceta, J.I., Wright, V.P., Pujalte, V., 2001. Palaeo-mixing zone karst features from Paleocene carbonates of north Spain: criteria for recognizing a potentially widespread but rarely documented diagenetic system. *Sedimentary Geology* 139, 205–216.

Barnolas, A., 1992. Evolución sedimentaria de la Cuenca Surpirenaica Oriental durante el Eoceno. *Acta geológica hispánica* 27, 15–31.

Barnolas, A., Gil-Peña, I., 2001. Ejemplos de relleno sedimentario multiepisódico en una cuenca de antepaís fragmentada: La Cuenca Surpirenaica. *Boletín Geológico y Minero* 112, 17-38.

Barnolas, A., Samsó, J.M., Teixell, A., Tosquella, J., Zamorano, M., 1991. Evolución sedimentaria entre la cuenca de Graus-Tremp y la cuenca de Jaca-Pamplona. In: Colombo, F. (Eds.), *I Congreso Del Grupo Español Del Terciario*, Guide Book 1, Vic, Spain, 123pp.

Bentham, P., Burbank, D.W., 1996. Chronology of Eocene foreland basin evolution along the western oblique margin of the South-Central Pyrenees. In: Friend, P.F., Dabrio, C.J. (Eds.), *Tertiary basins of Spain: the stratigraphic record of crustal kinematics*. Cambridge University Press, Cambridge, pp. 144–152.

Berastegui, X., Garcia-Senz, J.M., Losantos, M., 1990. Tecto-sedimentary evolution of the Organya extensional basin (central south Pyrenean unit, Spain) during the Lower Cretaceous. *Bulletin de la Société Géologique de France* VI, 251–264.

Berggren, W.A., 1995. A revised Cenozoic geochronology and chronostratigraphy. In: Berggren, W.A., Kent, D.V., Aubry, M.P., Hardenbol, J. (Eds), *Geochronology, time scales and global stratigraphic correlation*. SEPM (Society for Sedimentary Geology) Special Publication 54, Tulsa, pp. 129–212.

Bès de Berc, S., Soula, J.C., Baby, P., Souris, M., Christophoul, F., Rosero, J., 2005. Geomorphic evidence of active deformation and uplift in a modern continental wedge-top–foredeep transition: Example of the eastern Ecuadorian Andes. *Tectonophysics* 399, 351–380.

Bhattacharya, J.P., MacEachern, J.A., 2009. Hyperpycnal rivers and prodeltaic shelves in the Cretaceous seaway of North America. *Journal of Sedimentary Research* 79, 184-209.

Bond, R.M.G., McClay, K.R., 1995. Inversion of a Lower Cretaceous extensional basin, south central Pyrenees, Spain. In: Buchanan, J.G., Buchanan, P.G. (Eds), Basin inversion. Geological Society of London, Special Publications 88, pp. 415–431.

Bonini, M., Moratti, G., Sani, F., 1999. Evolution and depocentre migration in thrust-top basins: inferences from the Messinian Velona Basin (Northern Apennines, Italy). *Tectonophysics* 304, 95–108.

Bonorino, G.G., del Valle Abascal, L., 2012. Drainage and base-level adjustments during evolution of a late Pleistocene piggyback basin, Eastern Cordillera, Central Andes of northwestern Argentina. *Geological Society of America Bulletin* 124, 1858–1870.

Bown, T.M., Kraus, M.J., 1987. Integration of channel and floodplain suites, I. Developmental sequence and lateral relations of alluvial paleosols. *Journal of Sedimentary Research* 57, 587-601.

Brasier, M.D., 1975, The ecology and distribution of recent foraminifera from the reefs and shoals around Barbuda, West Indies. *Journal of Foraminiferal Research* 5, 193–210.

Brenchley, P.J., Romano, M., Gutiérrez-Marco, J.C., 1986. Proximal and distal hummocky cross-stratified facies on a wide Ordovician shelf in Iberia. Shelf Sands and Sandstones: In: Knight, R.J., McLean, J.R. (Eds.), *Canadian Society of Petroleum Geologists* 2, pp. 241–255.

Bridge, J.S., 1993. The interaction between channel geometry, water flow, sediment transport and deposition in braided rivers. In: Best, J.L., Bristow, C.S. (Eds.), *Braided Rivers*. Geological Society of London Special Publication 75, pp. 13–71.

Burbank, D.W., Beck, R.A., 1989. Early Pliocene uplift of the Salt Range; temporal constraints on thrust wedge development, northwest Himalaya, Pakistan. In: Malinconico, L.L., Jr., Lillie, R.J. (Eds.), *Tectonics of the western Himalayas*. Geological Society of America, Special Paper 232, pp. 113–128.

Burbank, D.W., Vergés, J., Muñoz, J.A., Bentham, P., 1992. Coeval hindward- and forward-imbricating thrusting in the south-central Pyrenees, Spain: Timing and rates of shortening and deposition. *Geological Society of America Bulletin* 104, 3–17.

Cant, D.J., Walker, R.G., 1978. Fluvial processes and facies sequences in the sandy braided South Saskatchewan River, Canada. *Sedimentology* 25, 625–648.

Casas, A.M., Soto, R., Martínez-Peña, B., 2002. Geometrical relationships between unconformities and subsequent folding: the Arro fold system (southern Pyrenees). *Comptes Rendus Géoscience* 334, 765–772.

Castelltort, S., Honegger, L., Adatte, T., Clark, J.D., Puigdefàbregas, C., Spangenberg, J.E., Dykstra, M.L., Fildani, A., 2017. Detecting eustatic and tectonic signals with carbon isotopes in deep-marine strata, Eocene Ainsa Basin, Spanish Pyrenees. *Geology* 45, 707–710.

Catuneanu, O., Abreu, V., Bhattacharya, J.P., Blum, M.D., Dalrymple, R.W., Eriksson, P.G., Fielding, C.R., Fisher, W.L., Galloway, W.E., Gibling, M.R., Giles, K. A., Holbrook, J.M., Jordan, R., Kendall, C.G.St.C., Macurda, B., Martinsen, O. J., Miall, A.D., Neal, J.E., Nummedal, D., Pomar, L., Posamentier, H.W., Pratt, B.R., Sarg,

J.F., Shanley, K.W., Steel, R.J.; Strasser, A., Tucker, M.E., Winker, C, 2009. Towards the standardization of sequence stratigraphy. *Earth-Science Reviews* 92, 1–33.

Charreau, J., Avouac, J.-P., Chen, Y., Dominguez, S., Gilder, S., 2008. Miocene to present kinematics of fault-bend folding across the Huerguosi anticline, northern Tianshan (China), derived from structural, seismic, and magnetostratigraphic data. *Geology* 36, 871–874.

Chiang, C.-S., Yu, H.-S., Chou, Y.-W., 2004. Characteristics of the wedge-top depozone of the southern Taiwan foreland basin system. *Basin Research* 16, 65–78.

Choukroune, P., Martinez, C., Séguret, M., Mattauer, M., 1968. Sur l'extension, le style et l'âge de mise en place de la nappe de Gavarnie (Pyrénées centrales). *Comptes Rendus de l'Académie des Sciences. Série D: Sciences Naturelles* 266, 1360–1363.

Cipollari, P., Cosentino, D., 1995. Miocene unconformities in the Central Apennines: geodynamic significance and sedimentary basin evolution. *Tectonophysics* 252, 375–389.

Clevis, Q., De Jager, G., Nijman, W., De Boer, P.L., 2004. Stratigraphic signatures of translation of thrust-sheet top basins over low-angle detachment faults. *Basin Research* 16, 145–163.

Conti, S., Fontana, D., Lucente, C.C., 2008. Sedimentary filling of a wedge-top basin and relationship with the foredeep (Middle Miocene Marnoso-arenacea Formation, northern Apennines). *Facies* 54, 479–498.

Cross, T.A., 1988. Controls on coal distribution in transgressive-regressive cycles, Upper Cretaceous Western Interior, U.S.A. In: Wilgus, C.K., Hastings, B.S., Ross, C.K., Posamentier, H.W., Van Wagoner, J., Kendall C.G.St.C. (Eds), *Sea-Level*

Changes - An Integrated Approach. Society of Economic Paleontologists and Mineralogists Special Publication 42, pp. 371–380

Crumeyrolle, P., 1987. Stratigraphie physique et sédimentologie des systèmes de dépôt de la séquence de Santa Liestra : Eocène sud-pyrénéen, Pyrénées aragonaises, Espagne. Thèse de Doctorat, Université de Bordeaux III.

Crumeyrolle, P., Lesueur, J.L., Claude, D., Joseph, P., 1992. Architecture et faciès d'un prisme deltaïque de bas niveau marin : les Grés de Roda (Bassin Eocène Sud Pyrénéen). Livret-guide de l'excursion ASF du 25-27 Septembre 1992. Publication ASF n°17, 76 pp.

Cuevas-Gozaló, M., Donselaar, M.E., Nio, S.D., 1985. Eocene clastic tidal deposits in the Tremp-Graus Basin (Provs. of Lérida and Huesca). In: Mila, M.D., Rosell, J. (Eds), 6th I.A.S. European Regional Meeting. Excursion Guidebook Excursion. Institut d'Estudis Illerdencs, Lleida, pp. 215–266.

Dalrymple, R.W., Zaitlin, B.A., Boyd, R., 1992. Estuarine facies models: conceptual basis and stratigraphic implications: perspective. *Journal of Sedimentary Research* 62, 1130-1146.

Davis Jr., R.A., Dalrymple R.W., 2012. Principles of tidal sedimentology. Springer, Berlin, Germany.

DeCelles, P.G., Giles, K.A., 1996. Foreland basin systems. *Basin Research* 8, 105–123.

Dott, R.J., Bourgeois, J., 1982. Hummocky stratification: Significance of its variable bedding sequences. *Geological Society of America Bulletin* 93, 663–680.

Dumas, S., Arnott, R.W.C., 2006. Origin of hummocky and swaley cross-stratification—the controlling influence of unidirectional current strength and aggradation rate. *Geology* 34, 1073–1076.

Eichenseer, H., 1988. Facies geology of late Maastrichtian to early Eocene coastal and shallow marine sediments, Tremp-Graus Basin, northeastern Spain. PhD thesis, University of Tübingen.

Eichenseer, H., Luterbacher, H., 1992. The marine Paleogene of the Tremp region (NE Spain)-depositional sequences, facies history, biostratigraphy and controlling factors. *Facies* 27, 119–151.

Elliott, T., 1976. Upper Carboniferous sedimentary cycles produced by river-dominated, elongate deltas. *Journal of the Geological Society* 132, 199–208.

Elliot, T., 1986. Deltas. In: Reading, H.G. (Ed.), *Sedimentary Environments and Facies*. Blackwell, Oxford, pp. 113–154.

Evans, M.J., Elliott, T., 1999. Evolution of a thrust-sheet-top basin: The Tertiary Barrême basin, Alpes-de-Haute-Provence, France. *Geological Society of America Bulletin* 111, 1617–1643.

Fernández, O., Muñoz, J.A., Arbués, P., Falivene, O., 2012. 3D structure and evolution of an oblique system of relaying folds: the Ainsa basin (Spanish Pyrenees). *Journal of the Geological Society* 169, 545–559.

Fernández, O., Muñoz, J.A., Arbués, P., Falivene, O., Marzo, M., 2004. Three-dimensional reconstruction of geological surfaces: An example of growth strata and turbidite systems from the Ainsa basin (Pyrenees, Spain). *American Association of Petroleum Geologists Bulletin* 88, 1049–1068.

Farrell, S.G., Williams, G.D., Atkinson, C.D., 1987. Constraints on the age of movement of the Montsec and Cotiella Thrusts, south central Pyrenees, Spain. *Journal of the Geological Society* 144, 907-914.

Ferrière, J., Reynaud, J.-Y., Migiros, G., Proust, J.-N., Bonneau, M., Pavlopoulos, A., Houze, A., 1998. Initiation d'un bassin transporté: l'exemple du « sillon méso-hellénique » au Tertiaire (Grèce). *Comptes Rendus de l'Académie des Sciences-Séries IIA-Earth and Planetary Science* 326, 567-574.

Ferrière, J., Reynaud, J.-Y., Pavlopoulos, A., Bonneau, M., Migiros, G., Chanier, F., Proust, J.-N., Gardin, S., 2004. Geologic evolution and geodynamic controls of the Tertiary intramontane piggyback Meso-Hellenic basin, Greece. *Bulletin de la Société Géologique de France* 175, 361-381.

Foix, N., Paredes, J.M., Giacosa, R.E., 2013. Fluvial architecture variations linked to changes in accommodation space: Río Chico Formation (late Paleocene), Golfo San Jorge basin, Argentina. *Sedimentary Geology* 294, 342-355.

Fonnesu, F., 1984. Estratigrafía física y análisis de facies de la secuencia de Figols entre el río Noguera Pallaresa e Iscles (Provs. De Lérida y Huesca). PhD Thesis, Universidad Autónoma de Barcelona.

Ford, M., 2004. Depositional wedge tops: interaction between low basal friction external orogenic wedges and flexural foreland basins. *Basin Research* 16, 361-375.

Friend, P.F., Hirst, J.P.P., Nichols, G.J., 1986. Sandstone-body structure and river process in the Ebro Basin of Aragón, Spain. *Cuadernos de Geología Ibérica* 10, 9-30.

Gaemers, P.A., 1978. Biostratigraphy, palaeoecology and palaeogeography of the mainly marine Ager Formation (Upper Paleocene—Lower Eocene) in the Tremp Basin, Central-South Pyrenees, Spain. *Leidse Geologische Mededelingen* 51, 151–215.

Galloway, W.E., 1989. Genetic stratigraphic sequences in basin analysis I: architecture and genesis of flooding-surface bounded depositional units. *American Association of Petroleum Geologists Bulletin* 73, 125–142.

Galloway, W.E., 1975. Process Framework for Describing the Morphologic and Stratigraphic Evolution of Deltaic Depositional Systems. In: Broussard, M.E. (Eds), *Deltas - Models for Exploration*. Houston Geological Society, Houston, Texas, pp. 87–98.

Galloway, W.E., Hobday, D.K., 1996. Terrigenous shelf systems. In: Galloway, W.E., Hobday, D.K. (Eds), *Terrigenous Clastic Depositional Systems*. Springer, Berlín, Heidelberg, pp. 159–185.

García Senz, J., 2002. Cuencas extensivas del Cretácico Inferior en los Pirineos centrales. Formación y subsecuente inversión. PhD thesis, Universitat de Barcelona.

Garrido-Megias, A., 1973. Estudio geológico y relación entre tectónica y sedimentación del secundario y terciario de la vertiente meridional pirenaica en su zona central (provincias de Huesca y Lérida). PhD thesis, University of Grenada.

Geel, T., 2000. Recognition of stratigraphic sequences in carbonate platform and slope deposits: empirical models based on microfacies analysis of Palaeogene deposits in southeastern Spain. *Palaeogeography, Palaeoclimatology, Palaeoecology* 155, 211–238.

Gertsch, B., Keller, G., Adatte, T., Berner, Z., Kassab, A.S., Tantawy, A.A.A., El-Sabbagh, A.M., Stueben, D., 2010. Cenomanian–Turonian transition in a shallow water sequence of the Sinai, Egypt. *International Journal of Earth Science* 99, 165–182.

Gradstein, F.M., Ogg, J.G., Schmitz, M., Ogg, G., 2012. *The Geologic Time Scale 2012*. Elsevier, Amsterdam.

Gugliotta, C., 2012. Inner vs. outer wedge-top depozone “sequences” in the Late Miocene (late Tortonian–early Messinian) Sicilian Foreland Basin System; new data from the Terravecchia Formation of NW Sicily. *Journal of Geodynamics* 55, 41–55.

Gugliotta, C., Gasparo Morticelli, M., 2012. Using high-resolution stratigraphy and structural analysis to constrain polyphase tectonics in wedge-top basins: Inferences from the late Tortonian Scillato Basin (central-northern Sicily). *Sedimentary Geology* 273–274, 30–47.

Hamon, Y., Deschamps, R., Joseph, P., Garcia, D., Chanvry, E., 2016. New insight of sedimentological and geochemical characterization of siliciclastic-carbonate deposits (Alveolina Limestone Formation, Graus-Tremp basin, Spain). *Bulletin de la Société Géologique de France* 187, 133–153.

Hardenbol, J., Thierry, J., Farley, M.B., Jacquin, T., de Graciansky, P.-C., Vail, P.R., 1998. Mesozoic and Cenozoic sequence chronostratigraphic framework of European basins. In: Graciansky, P.C, Hardenbol, J., Jacquin, T., Vail, P.R. (Eds.), *Mesozoic and Cenozoic sequence stratigraphy of European basins*. SEPM (Society for Sedimentary Geology) Special Publication, 60, pp. 3–13.

Heard, T.G., Pickering, K.T., 2008. Trace fossils as diagnostic indicators of deep-marine environments, Middle Eocene Ainsa-Jaca basin, Spanish Pyrenees. *Sedimentology* 55, 809–844.

Hermoza, W., Brusset, S., Baby, P., Gil, W., Roddaz, M., Guerrero, N., Bolaños, R., 2005. The Huallaga foreland basin evolution: Thrust propagation in a deltaic environment, northern Peruvian Andes. *Journal of South American Earth Sciences* 19, 21–34.

Homewood, P., Mauriaud, P., Lafont, F., 2000. Best Practices in Sequence Stratigraphy: For Explorationists and Reservoir Engineers. Bulletin Centre Recherche Elf Exploration Production, Mémoire 25, 81 pp.

Hottinger, L., 1960. Über paleocaene un eocaene Alveolinen. Doctoral dissertation, Verlag nicht ermittelbar.

Hottinger, L., Schaub, H., 1960. Zur Stufeneinteilung des Paleocaens und des Eocaens: Einführung der Stufen Ilerdien und Biarritzien. *Eclogae geologicae helvetiae* 53, 453-480.

Huerta, P., Armenteros, I., Silva, P.G., 2011. Large-scale architecture in non-marine basins: the response to the interplay between accommodation space and sediment supply. *Sedimentology* 58, 1716–1736.

Hwang, I.G., Chough, S.K., Hong, S.W., Choe, M.Y., 1995. Controls and evolution of fan delta systems in the Miocene Pohang Basin, SE Korea. *Sedimentary Geology* 98, 147–179.

Kraus, M.J., 1987. Integration of channel and floodplain suites, II. Vertical relations of alluvial paleosols. *Journal of Sedimentary Research* 57, 602-612.

Lafont, F., 1994. Influences relatives de la subsidence et de l'eustatisme sur la localisation et la geometrie des reservoirs d'un systeme deltaique. Exemple de l'Eocene du Bassin de Jaca, Pyrenees Espagnoles. Thèse de Doctorat, Université de Rennes 1.

Lawton, T.F., Trexler, J.H., 1991. Piggyback basin in the Sevier orogenic belt, Utah: Implications for development of the thrust wedge. *Geology* 19, 827–830.

Leckie, D.A., Walker, R.G., 1982, Storm- and tide dominated shorelines in Cretaceous Moosebar– Lower Gates interval—Outcrop equivalents of deep basin gas trap in Western Canada. *Bulletin of the American Association of Petroleum Geologists* 66, 138–157.

Leeder, M.R., Alexander, J., 1987. The origin and tectonic significance of asymmetrical meander-belts. *Sedimentology* 34, 217–226.

Leinfelder, R.R., Schmid, D.U., Nose, M., Werner, W., 2002. Jurassic reef patterns —the expression of a changing globe. In: Kiessling, W., Flügel, E., Golonka, J. (Eds.), *Phanerozoic Reef Patterns*. SEPM (Society for Sedimentary Geology) Special Publication 72, pp. 465–520.

Leren, B.L.S., Howell, J., Enge, H., Martinius, A.W., 2010. Controls on stratigraphic architecture in contemporaneous delta systems from the Eocene Roda Sandstone, Tremp-Graus Basin, northern Spain. *Sedimentary Geology* 229, 9–40.

Leturcq, T., 1999. Dynamique récifale à l'Ilerdien : exemple du bassin de Graus-Tremp (Pyrénées, Espagne). PhD thesis, Université Paris VI, France, 376 pp.

López-Blanco, M., Marzo, M., Muñoz, J.A., 2003. Low-amplitude, synsedimentary folding of a deltaic complex: Roda Sandstone (lower Eocene), South-Pyrenean Foreland Basin. *Basin Research* 15, 73–96.

Lucchi, F.R., 1986. The Oligocene to Recent foreland basins of the northern Apennines. In: Allen, P.A., Homewood, P. (Eds), *Foreland Basins*. Special Publication of the International Association of Sedimentologists 8. Blackwell Scientific Publication, Oxford, pp. 105-139.

Luterbacher, H.P., 1970. Environmental distribution of Early Tertiary microfossils, Tremp Basin, northeastern Spain. Esso Production Research–European Laboratories, Houston, Texas, 47 pp.

Maestro, E., 2008. Sedimentary evolution of the Late Eocene Vernet lacustrine system (South-Central Pyrenees). Tectono-climatic control in an alluvial-lacustrine piggyback basin. *Journal of Paleolimnology* 40, 1053-1078.

Martínez-Peña, M.B., 1991. La estructura del límite occidental de la Unidad Surpirenaica Central. PhD Thesis, Universidad de Zaragoza, Spain.

Martinius, A.W., 2012. Contrasting Styles of Siliciclastic Tidal Deposits in a Developing Thrust-Sheet-Top Basins – The Lower Eocene of the Central Pyrenees (Spain). In: Davis, R.A., Dalrymple, R.W. (Eds). *Principles of Tidal Sedimentology*. Springer, Netherlands, Dordrecht, pp. 473–506.

Martín-Martín, M., Martín-Algarra, A., 2002. Thrust sequence and syntectonic sedimentation in a piggy-back basin: the Oligo-Aquitania Mula–Pliego Basin (Internal Betic Zone, SE Spain). *Comptes Rendus Géoscience* 334, 363–370.

Marzo, M., Nijman, W., Puigdefabregas, C., 1988. Architecture of the Castissent fluvial sheet sandstones, Eocene, South Pyrenees, Spain. *Sedimentology* 35, 719–738.

Marzo, M., Steel, R.J., 2000. Unusual features of sediment supply-dominated, transgressive–regressive sequences: Paleogene clastic wedges, SE Pyrenean foreland basin, Spain. *Sedimentary Geology* 138, 3–15.

Mateu-Vicens, G., Pomar, L., Ferrandez-Canadell, C., 2012. Nummulitic banks in the upper Lutetian “Buil level”, Ainsa Basin, South Central Pyrenean Zone: the impact of internal waves. *Sedimentology* 59, 527–552.

Mazumder, R., Arima, M., 2005. Tidal rhythmites and their implications. *Earth-Science Reviews*. 69, 79–95.

Miall, A.D., 1977. A review of the braided-river depositional environment. *Earth-Science Reviews* 13, 1–62.

Miall, A.D., 1993. The architecture of fluvial-deltaic sequences in the upper Mesaverde Group (Upper Cretaceous), Book Cliffs, Utah. In: Best, J.L., Bristow, C.S. (Eds), *Braided Rivers*. Geological Society of London, Special Publications 75, pp. 305–332.

Mial, A.D., 1996. *The Geology of Fluvial Deposits*. Springer-Verlag, Berlin.

Minelli, N., Manzi, V., Roveri, M., 2013. The record of the Paleocene-Eocene thermal maximum in the Ager Basin (Central Pyrenees, Spain). *Geológica Acta* 11, 421–441.

Mitchum Jr., R.M., 1977. Seismic stratigraphy and global changes of sea level, part 11: glossary of terms used in seismic stratigraphy. In: Payton, C.E. (Eds), *Seismic Stratigraphy—Applications to Hydrocarbon Exploration*. American Association of Petroleum Geologists, Memoir 26, pp. 205–212.

Mochales, T., Barnolas, A., Pueyo, E.L., Serra-Kiel, J., Casas, A.M., Samsó, J.M., Ramajo, J., Sanjuán, J., 2012. Chronostratigraphy of the Boltaña anticline and the Ainsa Basin (southern Pyrenees). *Geological Society of America Bulletin* 124, 1229–1250.

Molenaar, N., 1990. Calcite cementation in shallow marine Eocene sandstones and constraints of early diagenesis. *Journal of the Geological Society* 147, 759–768.

Molenaar, N., Martinius, A.W., 1990. Origin of nodules in mixed siliciclastic-carbonate sandstones, the Lower Eocene Roda Sandstone Member, southern Pyrenees, Spain. *Sedimentary Geology* 66, 277–293.

Morley, C.K., Leong, L.C., 2008. Evolution of deep-water synkinematic sedimentation in a piggyback basin, determined from three-dimensional seismic reflection data. *Geosphere* 4, 939–962.

Morsilli, M., Bosellini, F.R., Pomar, L., Hallock, P., Aurell, M., Papazzoni, C.A., 2012. Mesophotic coral buildups in a prodelta setting (late Eocene, southern Pyrenees, Spain): a mixed carbonate–siliciclastic system. *Sedimentology* 59, 766–794.

Mugnier, J.L., Baby, P., Colletta, B., Vinour, P., Bale, P., Leturmy, P., 1997. Thrust geometry controlled by erosion and sedimentation: A view from analogue models. *Geology* 25, 427–430.

Mulder, T., Alexander, J., 2001. The physical character of subaqueous sedimentary density flows and their deposits. *Sedimentology* 48, 269–299.

Mulder, T., Syvitski, J.P., Migeon, S., Faugeres, J.-C., Savoye, B., 2003. Marine hyperpycnal flows: initiation, behavior and related deposits. A review. *Marine and Petroleum Geology* 20, 861–882.

Muñoz, J.A., 1992. Evolution of a continental collision belt: ECORS-Pyrenees crustal balanced cross-section. In: Mc Clay, K. (Eds), *Thrust Tectonics*. Springer, Dordrecht, pp. 235–246.

Muñoz, J.-A., Beamud, E., Fernández, O., Arbués, P., Dinarès-Turell, J., Poblet, J., 2013. The Ainsa Fold and thrust oblique zone of the central Pyrenees: Kinematics of a curved contractional system from paleomagnetic and structural data. *Tectonics* 32, 1142–1175.

Muñoz, J.A., McClay, K., Poblet, J., 1994. Synchronous extension and contraction in frontal thrust sheets of the Spanish Pyrenees. *Geology* 22, 921–924.

Mutti, E., Normark, W.R., 1987. Comparing Examples of Modern and Ancient Turbidite Systems: Problems and Concepts. In: Leggett, J.K., Zuffa, G.G. (Eds.), *Marine Clastic Sedimentology*. Springer, Dordrecht, pp. 1–38.

Mutti, E., Séguret, M., Sgavetti, M., 1988. Sedimentation and deformation in the Tertiary Sequences of the Southern Pyrenees. AAPG Mediterranean Basin Conference Special Publication, September 1988, Field trip no 7, Parma: Institute of Geology, University of Parma, 153 pp.

Mutti, E., Sgavetti, M., Waehry, A., Carminatti, M., Davoli, G., Ghielmi, M., Fighi, M., Mora, S., 1994. Regional stratigraphy and sequence-stratigraphic aspects of the Figols Group. In: Mutti, E., Davoli, G., Mora, S., Sgavetti, M. (Eds), *The Eastern Sector of the South-Central Folded Pyrenean Foreland: Criteria for Stratigraphic Analysis and Excursion Notes*. Second High-Resolution Sequence Stratigraphic Conference, Tremp, Spain. Institute Geologica, Parma University, Italy, pp. 37–41.

Mutti, E., Tinterri, R., Benevelli, G., Biase, D., Cavanna, G., 2003. Deltaic, mixed and turbidite sedimentation of ancient foreland basins. *Marine and Petroleum Geology* 20, 733–755.

Mutti, E., Tinterri, R., Di Biase, D., Fava, L., Mavilla, N., Angella, S., Calabrese, L., 2000. Delta-Front Facies Associations of Ancient Flood-Dominated Fluvio-Deltaic System. *Revista Sociedad Geológica de España* 13, 165-190.

Nijman, W., 1998. Cyclicity and basin axis shift in a piggyback basin: towards modelling of the Eocene Tremp-Ager Basin, South Pyrenees, Spain. In: Mascle, A., Puigdefabregas, C., Luterbacher, H.P., Fernandez M. (Eds), *Cenozoic Foreland Basin of Western Europe*. Geological Society of London, Special Publications 134, pp. 135–162.

Nijman, W., Nio, S., 1975. The Eocene Montañana delta (Tresp-Graus Basin, provinces of Lerida and Huesca, southern Pyrenees, N. Spain). In: Rosell, J., Puigdefabregas, C. (Eds), Sedimentary evolution of the Paleogene South Pyrenean Basin, Part B, IAS 9th International Congress, Nice, pp. 29–87.

Nio, S.D., Yang, C.S., 1991. Sea-level fluctuations and the geometric variability of tide-dominated sandbodies. *Sedimentary Geology* 70, 161–193.

O'Brien, P.E., Wells, A.T., 1986. A Small, Alluvial Crevasse Splay. *Journal of Sedimentary Research*. 56, 876-879.

Odgaard, A.J., 1989. River-meander model. I: Development. *Journal of Hydraulic Engineering* 115, 1433-1450.

Olariu, M.I., Olariu, C., Steel, R.J., Dalrymple, R.W., Martinius, A.W., 2012. Anatomy of a laterally migrating tidal bar in front of a delta system: Esdolomada Member, Roda Formation, Tresp-Graus Basin, Spain. *Sedimentology* 59, 356–378.

Olivero, E.B., Ponce, J.J., Martinioni, D.R., 2008. Sedimentology and architecture of sharp-based tidal sandstones in the upper Marambio Group, Maastrichtian of Antarctica. *Sedimentary Geology* 210, 11–26.

Ori, G.G., Friend, P.F., 1984. Sedimentary basins formed and carried piggyback on active thrust sheets. *Geology* 12, 475–478.

Orton, G.J., Reading, H.G., 1993. Variability of deltaic processes in terms of sediment supply, with particular emphasis on grain size. *Sedimentology* 40, 475–512.

Olariu, C., Steel, R.J., Petter, A.L., 2010. Delta-front hyperpycnal bed geometry and implications for reservoir modeling: Cretaceous Panther Tongue delta, Book Cliffs, Utah. *American Association of Petroleum Geologists Bulletin* 94, 819–845.

Payros, A., Pujalte, V., Baceta, J.I., Bernaola, G., Orue Etxebarria, X., Apellaniz, E., Caballero, E., Ferrandez, C., 2000. Lithostratigraphy and Sequence Stratigraphy of the Upper Thanetian to Middle Illerdian strata of the Campo Section (Southern Pyrenees, Spain): revision and new data. *Revista Sociedad Geológica de España*, 2, 213-226.

Payros, A., Tosquella, J., Bernaola, G., Dinarès-Turell, J., Orue-Etxebarria, X., Pujalte, V., 2009. Filling the North European Early/Middle Eocene (Ypresian/Lutetian) boundary gap: Insights from the Pyrenean continental to deep-marine record. *Palaeogeography, Palaeoclimatology, Palaeoecology* 280, 313–332.

Pemberton, S.G., Wightman, D.M., 1992. Ichnological characteristics of brackish water deposits. In: Pemberton S.G. (Ed.), *Applications of Ichnology to Petroleum Exploration*. SEPM Core Workshop 17, pp. 141–167.

Peper, T., de Boer, P.L., 1995. Intrabasinal thrust-tectonic versus climate control on rhythmicities in the Eocene South Pyrenean Tremp-Graus foreland basin: inferences from forward modelling. *Tectonophysics* 249, 93–107.

Petter, A.L., Steel, R.J., 2006. Hyperpycnal flow variability and slope organization on an Eocene shelf margin, Central Basin, Spitsbergen. *American Association of Petroleum Geologists Bulletin* 90, 1451–1472.

Pickering, K.T., Bayliss, N.J., 2009. Deconvolving tectono-climatic signals in deep-marine siliciclastics, Eocene Ainsa basin, Spanish Pyrenees: Seesaw tectonics versus eustasy. *Geology* 37, 203–206.

Pivnik, D.A., Khan, M.J., 1996. Transition from foreland-to piggyback-basin deposition, Plio-Pleistocene Upper Siwalik Group, Shinghar Range, NW Pakistan. *Sedimentology* 43, 631–646.

Plaziat, J.-C., 1981. Late Cretaceous to late Eocene palaeogeographic evolution of southwest Europe. *Palaeogeography, Palaeoclimatology, Palaeoecology* 36, 263–320.

Plink-Björklund, P., Steel, R.J., 2004. Initiation of turbidity currents: outcrop evidence for Eocene hyperpycnal flow turbidites. *Sedimentary Geology* 165, 29–52.

Pomar, L., 2001. Types of carbonate platforms: a genetic approach. *Basin Research* 13, 313–334.

Posamentier, H.W., Vail, P.R., 1988. Eustatic controls on clastic deposition I—conceptual framework. In: Wilgus, C.K., Hastings, B.S., Ross, C.K., Posamentier, H.W., Van Wagoner, J., Kendall C.G.St.C. (Eds), *Sea-Level Changes-An Integrated Approach*. Society of Economic Paleontologist and Mineralogists Special Publication 42, pp. 125-154.

Postma, G., Drinia, H., 1993. Architecture and sedimentary facies evolution of a marine, expanding outer-arc half-graben (Crete, late Miocene). *Basin Research* 5, 103–124.

Poyatos-Moré, M., 2014. *Physical Stratigraphy and Facies Analysis of the Castissent Tecto-Sedimentary Unit (South-Central Pyrenees, Spain)*. PhD thesis, Universidad Autónoma de Barcelona.

Puigdefàbregas, C., Muñoz, J.A., Vergés, J., 1992. Thrusting and foreland basin evolution in the Southern Pyrenees. In: Mc Clay, K. (Eds), *Thrust Tectonics*. Springer, Dordrecht, pp. 247–254.

Puigdefàbregas, C., Souquet, P., 1986. Tecto-sedimentary cycles and depositional sequences of the Mesozoic and Tertiary from the Pyrenees. *Tectonophysics* 129, 173–203.

Puigdefàbregas, C., Van Vliet, A., 1978. Meandering stream deposits from the Tertiary of the southern Pyrenees. In Miall, A.D. (Ed.), *Fluvial sedimentology*: Canadian Society of Petroleum Geologists Memoir 5, pp. 469–485.

Pujalte, V., Schmitz, B., Baceta, J.I., Orue Etxebarria, X., Bernaola, G., Dinarès-Turell, J., Payros, A., Apellaniz, E., Caballero, E., 2009. Correlation of the Thanetian-Illerdian turnover of larger foraminifera and the Paleocene-Eocene thermal maximum: confirming evidence from the Campo area (Pyrenees, Spain). *Geológica Acta* 7, 161–175.

Pujalte, V., Baceta, J. I., Schmitz, B., Orue-Etxebarria, X., Payros, A., Bernaola, G., Apellaniz, E., Caballero, F., Robador, A., Serra-Kiel, J., Tosquella, J., 2009b. Redefinition of the Illerdian stage (early Eocene). *Geológica Acta* 7, 117-194.

Pujalte, V., Schmitz, B., Baceta, J.I., 2014. Sea-level changes across the Paleocene–Eocene interval in the Spanish Pyrenees, and their possible relationship with North Atlantic magmatism. *Palaeogeography, Palaeoclimatology, Palaeoecology* 393, 45–60.

Ramos, E., Busquets, P., Vergés, J., 2002. Interplay between longitudinal fluvial and transverse alluvial fan systems and growing thrusts in a piggyback basin (SE Pyrenees). *Sedimentary Geology* 146, 105–131.

Ramos, A., Sopena, A., 1983. Gravel bars in low-sinuosity streams (Permian and Triassic, central Spain). In: Collison, J.D., Lewin, J. (Eds.), *Modern and Ancient Fluvial Systems*. International Association of Sedimentologist Special Publication 6, pp. 301-313.

Rasser, M.W., Scheibner, C., Mutti, M., 2005. A paleoenvironmental standard section for Early Ilerdian tropical carbonate factories (Corbieres, France; Pyrenees, Spain). *Facies* 51, 218–232.

Remacha, E., Fernández, L.P., 2003. High-resolution correlation patterns in the turbidite systems of the Hecho Group (South-Central Pyrenees, Spain). *Marine and Petroleum Geology* 20, 711–726.

Remacha, E., Zamorano, M., 1989. Reflejo de la estratigrafía secuencial del Eoceno inferior surpirenaico en una parte de la sección de Campo. *Geogaceta* 6, 94–96.

Riba, O., 1976. Syntectonic unconformities of the Alto Cardener, Spanish Pyrenees: a genetic interpretation. *Sedimentary Geology* 15, 213–233.

Rosell, J., Linares, R., Llompart, C., 2001. El “Garumniense” prepirenaico. *Revista de la Sociedad Geológica de España* 14, 47–56.

Rossi, M., Rogledi, S., Barbacini, G., Casadei, D., Iaccarino, S., Papani, G., 2002. Tectono-stratigraphic architecture of Messinian piggyback basins of Northern Apennines: the Emilia folds in the Reggio-Modena area and comparison with the Lombardia and Romagna sectors. *Bollettino della Società Geologica Italiana* 1, 437–447.

Roure, F., 2008. Foreland and Hinterland basins: what controls their evolution? *Swiss Journal of Geosciences* 101, 5–29.

Roure, F., Choukroune, P., Berastegui, X., Munoz, J.A., Villien, A., Matheron, P., Bareyt, M., Séguret, M., Camara, P., Deramond, J., 1989. ECORS deep seismic data and balanced cross sections: Geometric constraints on the evolution of the Pyrenees. *Tectonics* 8, 41–50.

Samsó, J.M., Tosquella, J., Serra-Kiel, J., 1990. Los géneros *Alveolina* y *Nummulites* (Macroforaminíferos) del Ilerdense Medio-Cuisense Medio de la Cuenca de Graus, Huesca. I. Sistemática de *Alveolina*. *Boletín Geológico y Minero* 101, 219–252.

Schmitz, B., Pujalte, V., 2003. Sea-level, humidity, and land-erosion records across the initial Eocene thermal maximum from a continental-marine transect in northern Spain. *Geology* 31, 689-692.

Schmitz, B., Pujalte, V., 2007. Abrupt increase in seasonal extreme precipitation at the Paleocene-Eocene boundary. *Geology* 35, 215-218.

Scheibner, C., Rasser, M.W., Mutti, M., 2007. The Campo section (Pyrenees, Spain) revisited: Implications for changing benthic carbonate assemblages across the Paleocene–Eocene boundary. *Palaeogeography, Palaeoclimatology, Palaeoecology* 248, 145-168.

Séguret, M., 1972. Étude tectonique des nappes et séries décollées de la partie centrale des Pyrénées. Thèse de Doctorat, Université de Montpellier.

Serra-Kiel, J., Canudo, J.I., Dinares, J., Molina, E., Ortiz, N., Pascual, J.O., Samsó, J.M., Tosquella, J., 1994. Cronoestratigrafía de los sedimentos marinos del Terciario inferior de la Cuenca de Graus-Tremp (Zona Central Surpirenaica). *Revista de la Sociedad Geológica de España* 7, 273–297.

Serra-Kiel, J., Hottinger, L., Caus, E., Drobne, K., Ferrandez, C., Jauhri, A.K., Less, G., Pavlovec, R., Pignatti, J., Samsó, J.M., Schaub, H., Sirel, E., Strougo, A., Tambareau, Y., Tosquella, J., Zakrevskaya E., 1998. Larger foraminiferal biostratigraphy of the Tethyan Paleocene and Eocene. *Bulletin de la Société géologique de France* 169, 281–299.

Sgavetti, M., 1992. Criteria for Stratigraphic Correlation Using Aerial Photographs: Examples from the South-Central Pyrenees (1). *American Association of Petroleum Geologists Bulletin* 76, 708–730.

Shanley, K.W., McCabe, P.J., Hettinger, R.D., 1992. Tidal influence in Cretaceous fluvial strata from Utah, USA: a key to sequence stratigraphic interpretation. *Sedimentology* 39, 905–930.

Sinclair, H.D., Allen, P.A., 1992. Vertical versus horizontal motions in the Alpine orogenic wedge: stratigraphic response in the foreland basin. *Basin Research* 4, 215–232.

Smith, N.D., Cross, T.A., Dufficy, J.P., Clough, S.R., 1989. Anatomy of an avulsion. *Sedimentology* 36, 1–23.

Sohn, Y.K., Rhee, C.W., Kim, B.C., 1999. Debris flow and hyperconcentrated flood-flow deposits in an alluvial fan, northwestern part of the Cretaceous Yongdong basin, central Korea. *The Journal of Geology*, 107, 111–132.

Soler-Sampere, M., Garrido-Megías, A., 1970. La terminación occidental del manto de Cotiella. *Pirineos* 98, 5-12.

Soto, R., Casas, A.M., Storti, F., Faccenna, C., 2002. Role of lateral thickness variations on the development of oblique structures at the Western end of the South Pyrenean Central Unit. *Tectonophysics* 350, 215-235.

Suriano, J., Limarino, C.O., Tedesco, A.M., Alonso, M.S., 2015. Sedimentation model of piggyback basins: Cenozoic examples of San Juan Precordillera, Argentina. In: Sepúlveda, S.A., Giambiagi, L.B., Moreiras, S.M., Pinto, L., Tunik, M., Hoke, G.D., Farías, M. (Eds.), *Geodynamic Processes in the Andes of Central Chile and Argentina*. Geological Society of London, Special Publications 399, pp. 221–244.

Talling, P.J., Lawton, T.F., Burbank, D.W., Hobbs, R.S., 1995. Evolution of latest Cretaceous–Eocene nonmarine deposystems in the Axhandle piggyback basin of central Utah. *Geological Society of America Bulletin* 107, 297–315.

Teixell, A., Muñoz, J.A., 2000. Evolución tectonosedimentaria del Pirineo meridional durante el Terciario: una síntesis basada en la transversal del río Noguera Ribagorçana. *Revista de la Sociedad Geológica de España* 13, 251–264.

Thomas, R.G., Smith, D.G., Wood, J.M., Visser, J., Calverley-Range, E.A., Koster, E.H., 1987. Inclined heterolithic stratification—terminology, description, interpretation and significance. *Sedimentary Geology* 53, 123–179.

Tinterri, R., 2007. The Lower Eocene Roda Sandstone (South-Central Pyrenees): An Example of a Flood-Dominated River-Delta System in a Tectonically Controlled Basin. *Rivista Italiana di Paleontologia e Stratigrafia (Research In Paleontology and Stratigraphy)* 113, 223-255.

Tosquella, J., 1988. Estudi Sedimentològic i Biostratigràfic de la Formació Gresos de Roda (Eoceno Conca Tremp-Graus). Unpublished M.Sc. thesis, University of Barcelona, Barcelona.

Tosquella, J., Samsó, J.M., Serra-Kiel, J., 1990. Los géneros *Alveolina* y *Nummulites* (Macroforaminíferos) del Ilerdense Medio-Cuisiense Medio de la Cuenca de Graus, Huesca. II. Sistemática de *Nummulites*. *Boletín Geológico y Minero* 101, 351–403.

Tosquella, J., Serra-Kiel, J., Ferrandez-Canadell, C., Samsó, J.M., 1996. Las biozonas de nummulíticos del Paleoceno Superior-Eoceno Inferior de la Cuenca Pirenaica. *Acta geológica hispánica* 31, 23–36.

Vail, P.R., Audemard, F., Bowman, S.A., Eisner, P.N., Perez-Cruz, C., 1991. The stratigraphic signatures of tectonics, eustasy and sedimentology: an overview. In: Einsele, G., Ricken, W., Seilacher, A. (Eds), *Cycles and Events in Stratigraphy*, Springer-Verlag. New York, Berlin, pp. 617–659.

Vail, P.R., Mitchum Jr, R.M., Thompson III, S., 1977. Seismic stratigraphy and global changes of sea level: Part 3. Relative changes of sea level from Coastal Onlap. In: Payton, C.W., (Eds), *Seismic Stratigraphy—Applications to Hydrocarbon Exploration*. American Association of Petroleum Geologists Memoir 26, pp. 83-97.

Van Der Meulen, S., 1983. Internal structure and environmental reconstruction of Eocene transitional fan-delta deposits, Montllobat-Castigaleu formations, Southern Pyrenees, Spain. *Sedimentary Geology* 37, 85–112.

Van Wagoner, J.C., Posamentier, H.W., Mitchum, R.M., Vail, P.R., Sarg, J.F., Loutit, T.S., Hardenbol, J., 1988. An overview of sequence stratigraphy and key definitions. In: Wilgus, C.K., Hastings, B.S., Ross, C.K., Posamentier, H.W., Van Wagoner, J., Kendall C.G.St.C. (Eds), *Sea-Level Changes-An Integrated Approach*. Society of Economic Paleontologist and Mineralogists, Special Publication 42, pp. 39-45.

Vera, J.A., (Ed.), 2004. *Geología de España*. SGE-IGME, Madrid.

Vergés, J., 1993. *Estudi geològica del vessant sud del Pirineu oriental i central. Evolució cinemàtica en 3D*. PhD thesis, University of Barcelona.

Vergés, J., 2009. Drainage responses to oblique and lateral thrust ramps: a review. In: Nichols, G.G., Paola, C. Williams, E. (Eds) *Sedimentary Processes, Environments and Basins: A Tribute to Peter Friend*. International Association of Sedimentologists, Special Publication 38, pp. 29–47.

Vergés, J., 2003. Evolución de los sistemas de rampas oblicuas de los Pirineos meridionales: fallas del Segre y Pamplona. *Boletín Geológico y Minero de España*. 114, 87–101

Vincent, S.J., 2001. The Sis palaeovalley: a record of proximal fluvial sedimentation and drainage basin development in response to Pyrenean mountain building. *Sedimentology* 48, 1235–1276.

Vincent, S.J., Elliott, T., 1997. Long-lived transfer zone paleovalleys in mountain belts: an example from the Tertiary of the Spanish Pyrenees. *Journal of Sedimentary Research* 67, 303-310.

Walker, R.G., 1985. Mudstones and thin-bedded turbidites associated with the Upper Cretaceous Wheeler Gorge conglomerates, California: a possible channel-levee complex. *Journal of Sedimentary Research* 55, 279-290.

Weltje, G.J., Van Ansenwoude, S., De Boer, P.L., 1996. High-frequency detrital signals in Eocene fan-delta sandstones of mixed parentage (south-central Pyrenees, Spain): a reconstruction of chemical weathering in transit. *Journal of Sedimentary Research* 66, 119-131.

Wheeler, D.M., Scott, A.J., Coringrato, V.J., Devine, P.E., 1990. Stratigraphy and Depositional History of the Morrow Formation, Southeast Colorado and Southwest Kansas. In: Sonnenberg, S.A., Shannon, L.T., Rader, K., von Drehle, W.F., Martin, G.W. (Eds.), *Morrow Sandstones of Southeast Colorado and Adjacent Areas*. The Rocky Mountain Association of Geologists, pp. 3–35.

Whitchurch, A.L., Carter, A., Sinclair, H.D., Duller, R.A., Whittaker, A.C., Allen, P.A., 2011. Sediment routing system evolution within a diachronously uplifting

orogen: Insights from detrital zircon thermochronological analyses from the South-Central Pyrenees. *American Journal of Science* 311, 442–482.

Williams, P.F., Rust, B.R., 1969. The sedimentology of a braided river. *Journal of Sedimentary Research* 39, 649-679.

Wright, V.P., Burchette, T.P., 1998. Carbonate ramps: an introduction. In: Wright, V.P., Burchette, T.P. (Eds), *Carbonate Ramps*. Geological Society of London, Special Publications 149, pp. 1–5.

Yang, C.S., Nio, S.D., 1985. The estimation of palaeohydrodynamic processes from subtidal deposits using time series analysis methods. *Sedimentology* 32, 41–57.

Yang, C.-S., Nio, S.-D., 1989. An ebb-tide delta depositional model—a comparison between the modern Eastern Scheldt tidal basin (southwest Netherlands) and the Lower Eocene Roda Sandstone in the southern Pyrenees (Spain). *Sedimentary Geology* 64, 175–196.

Zapata, T.R., Allmendinger, R.W., 1996. Growth stratal records of instantaneous and progressive limb rotation in the Precordillera thrust belt and Bermejo basin, Argentina. *Tectonics* 15, 1065–1083.

Zoetemeijer, R., Cloetingh, S., Sassi, W., Roure, F., 1993. Modelling of piggyback-basin stratigraphy: record of tectonic evolution. *Tectonophysics* 226, 253–269.

Figure captions

Fig. 1. Sketch showing regional (green) versus local (blue) controls on sediment supply (S) and accommodation (A) in a piggyback basin.

Fig. 2. (a) The South Pyrenean Central Unit in the South Pyrenean Zone (To: Toulouse; Le: Lerida; Hu: Huesca; Pa: Pamplona). (b) Structural map of the South Pyrenean Central Unit showing the main cover and basement units. (c) Regional composite syn-orogenic lithostratigraphy showing the sedimentary succession along the Isabena valley in the Tremp-Graus Basin. (d) structural cross-section through the South Pyrenean Central Unit (Muñoz, 1992)

Fig. 3. Geological map of the Tremp-Graus-Ainsa Basin compiled from IGME and the geological map of Cataluña 1/250000. Structural features in the Isabena area and the Boixols thrust are from Lopez-Blanco et al. (2003) and Ardèvol et al. (2000). Coll del Vent anticline location is from Vincent (2001). Red structures are considered as active during the studied interval (Ypresian). Location of measured sedimentological sections is shown in thick white line.

Fig. 4. Chrono-litho- stratigraphic diagrams of the Tremp-Graus-Ainsa Basin during the Paleocene-Eocene times. The tectonic events are compiled from Fernandez et al. (2012) and Muñoz et al. (2013). Stratigraphy is compiled from Nijman and Nio (1975); Mutti et al. (1988); Serra-Kiel et al. (1994); Barnolas and Gil-Pena (2001); Muñoz et al. (2013); Lopez-Blanco et al. (2003) and Vera (2004). Colors of the stratigraphic units indicated in Fig. 2. Polarity chrons is from the GTS 2012 (Gradstein et al., 2012). Planktonic foraminifera biozones from Berggren et al. (1995), with revised age calibration updates. The Tethyan Shallow Benthic Zones are from Hardenbol et al. (1998), and updated by GTS2012 Paleogene chapter group. Calcareous nannofossils Martini NP and Burky CP zones are from Berggren (1995). S.M.P.P: Suerri, Mur-

Puigvert and Porredo systems (Fonnesu, 1984); At.: Atiart unconformity; Ch-La: Charo2-Lacorz unconformity.

Fig. 5. Facies associations observed in the Lower Eocene of the Tremp-Graus-Ainsa basin.

Fig. 6. (a) Alluvial stream flow fan; Cg: Conglomeratic facies; VCS: intercalation of very coarse sandstones with through cross bedding; MS: Medium sandstone on top of sequence (FA1, Montllobat Fm.); (b) Multistorey braided channel belt, with a detail view of through cross bedding in coarse sandstone (FA2.1, Castissent Fm.); (c) Meandering channel fill with a detail view of lateral accreting bed (FA3, Montllobat Fm.); (d) Delta plain deposits with erosive-based and fining-up subaqueous distributary channel with a detail view on through cross bedding (FA5, Castigaleu Fm.); (e) Tidal channel with detail view of flaser bedding (FA7, Castigaleu Fm.); (f) High angle fluvial dominated Gilbert delta (FA6.1, Roda Sandstone, Isabena Valley section); (g) Low angle fluvial dominated delta front with thickening upward sequence (FA6.2, Castissent Fm.); (h) Subtidal bar (FA9; Roda Sandstone); (i) Low angle tide dominated delta front deposits (FA9; Castigaleu Fm.); (j) Inner carbonate platform thin section with *Alveolina* (Al.), *Orbitolitids* (Or.) and *Miliolids* (Mi.); (FA10, *Alveolina* Limestone); (k) Silty prodelta with coarsening upward sequence, detail view of hyperpycnite deposit (FA13, Castissent Fm.); (l) Shelfal turbidite succession (FA14, Castissent Fm.); (m) Iscles reef (*Alveolina* Limestone); (n) Field photography of coral dominated reef and (o) in thin section; (*Alveolina* Limestone); (p) Detail on *Solenomeris* dominated reef environment (*Alveolina* Limestone); (q) Mid carbonate platform (FA11; Morillo Limestone) and (r)

thin section of a packstone with Nummulites (Num.), Miliolids (Mi.), Alveolina (Al.), Orbitolitids (Or.) faunal assemblage; (s) Mid to outer carbonate platform with thickening upward sequence (FA11, La Puebla Limestone, and (t) associate thin section of a packstone with Assilinids dominated faunal assemblage; (u) Slope deposits with alternation of slumped facies (FA16) and thin bedded turbidites (FA17.1: San Vicente Fm.); (v) Atiart submarine erosional surface with onlapping slope deposits (Castigaleu/San Vicente Fms.); (w) Amalgamated turbidite channel facies interbedded with debris flow deposits (Df.) (FA17.2: Fosado Channel).

Fig. 7. (a-d): Summary block diagrams of depositional systems and forming facies associations. (e) General profile showing the partitioning of all of the depositional environments from a proximal area to a distal position within the basin.

Fig. 8. Wheeler diagram of the Graus-Tremp-Ainsa Basin, with age model, showing the time relationships between stratigraphic sequences, stratigraphic surfaces and depositional environment partitioning. Vertical axis is unscaled, i.e., each Short Term Sequence is represented with a same interval range as the others.

Fig. 9. Summarized stratigraphic sections in eastern part of the Tremp-Graus-Ainsa Basin (South Ribagorzana and Montañana), with interpreted depositional environment and stacking pattern. Stratigraphic surfaces according to the proposed sequences order are based on proximal (A) to distal (K) vertical evolution of depositional environments.

Fig. 10. Summarized stratigraphic section along the central part of the Tremp-Graus-Ainsa Basin (Isabena Valley) with interpreted depositional environment and stacking pattern. Stratigraphic surfaces for the proposed sequences order are based on the vertical stacking of depositional environments. Larger benthic foraminifera (SBZ) biozones are from Serra Kiel et al. (1994). Legend of depositional environment colors indicated in Fig. 9.

Fig. 11. Summarized stratigraphic sections in the western part of the Tremp-Graus-Ainsa Basin (Atiart and Campo) with interpreted depositional environment and stacking pattern. Stratigraphic surfaces for the proposed sequences order are based on the vertical stacking of the depositional environments. Larger benthic foraminifera (SBZ) biozones are from Serra Kiel et al. (1994). Legend of depositional environment colors indicated in Fig. 9.

Fig. 12. Stratigraphic correlation across the Tremp-Graus-Ainsa basin during Ypresian times; (a) Stratigraphic surfaces with two major orders of sequences defined (thin and thick sequence boundaries); (b) Facies association distribution within the correlation transect.

Fig. 13. (a-d) Paleogeographic reconstructions of the Tremp-Graus-Ainsa Basin during Ypresian. Active structural events are indicated for each map and (e) synthesized for each Depositional Sequence. Major paleocurrents directions indicated after removing of rotation effect (see Appendix B for detail paleocurrent measurement). Maps are reconstructed in palinspastic position according to Muñoz et al. (2013). The location of

active tectonic structures such as the Atiart thrust, Foradada fault and Montsec placed according to Muñoz et al. 2013. Bóixols thrust, Coll del Vent Anticline and Roda folds from López-Blanco et al. (2013). Luzàs fault from Nijman (1989). Sedimentary data and paleocurrent directions are from own field data. Section abbreviations are given in Fig. 3.

Fig. 14. Correlation transects restored in syn-sedimentary position, by flattening the top MFS (TE1 to TE3) and the top TS (TE4). The inferred active structures are indicated.

Fig. 15. Summarized model specific to a piggyback basin evolution. The Stratigraphic surfaces for the proposed sequences from (a) Gugliotta and Morticelli (2012) and (b) Evans and Elliott (1999) are based on the vertical stacking of depositional environments and compared to (c) the Graus-Tremp sub-basin. Refer to Fig. 9 for color legend of depositional environments. In the Barrême Basin succession; PA=Poudingues d'Argens ; CN : Calcaires Nummulitiques ; MB : Marnes Bleues ; GdV : Grès de Ville ; CdC : Conglomérats de Clumanc ; CdSL : Conglomérats de St Lions ; MR : Molasse Rouge ; SS : Série Saumon ; SG : Série Grise ; GV : Grès Verts.

Tables

Table 1. Summary of the Tremp-Graus-Ainsa Basin lithostratigraphy with Formation names, age, some particularities and previous works associated.

Age	Formation	Particularity	References
Paleocene	Garumnian Facies, Tremp Formation	Continental "red bed"	Eichenseer and Luterbacher, 1992; Rosell et al., 2001
	Navarri Formation	Shallow water carbonates	Scheibner et al., 2007
Paleocene / Eocene transition	Claret Conglomerate	Braidplain deposits (eastern part) passing to fluvial channels, settled during PETM	Schmitz and Pujalte, 2007; Pujalte et al., 2009; Minelli et al., 2013; Pujalte et al., 2014
Ypresian (lower Illeridian)	Alveolina Limestone	Shallow marine carbonate + Berganuy, Iscles and Merli reef systems	Fonnesu, 1984; Eichenseer, 1988; Mutti et al., 1988; Eichenseer and Luterbacher, 1992; Leturcq, 1999; Payros et al., 2000; Baceta et al., 2001; Hamon et al., 2016
	- Riguala Marls Formation - La Puebla Limestone	- Nummulite-rich marls - macroforaminifera-rich carbonates	Cuevas-Gozaló et al., 1985; Remacha and Zamorano, 1989

Ypresian (upper Illeridian / lower Cuisian)	Roda Sandstone	Deltaic systems	Yang and Nio, 1985; Yang and Nio, 1989; Eichenseer, 1988; Tosquella, 1988; Molenaar, 1990; Crumeyrolle et al., 1992; López-Blanco et al., 2003; Leren et al., 2010; Olariu et al., 2012
	Upper Detritic Complex	Deltaic systems	Tosquella 1988
	Suerri, Mur-Puigvert and Poreredo systems	Deltaic and tide systems	Fonnesu, 1984
	Morillo Limestone	Foraminifera rich carbonates	Nijman and Nio, 1975; Cuevas-Gozalo et al., 1985
Ypresian (lower Cuisian)	Lower Montanana Group: - San Esteban Fm. - Montllobat Fm. - Castigaleu Fm.	- Alluvial Fan - Fluvial env. - Delta plain to shallow-marine env.	Nijman and Nio, 1975; Van Der Meulen, 1983; Mutti et al., 1988; Nijman, 1998
Ypresian (middle Cuisian)	Middle Montanana Group: - Castissent Fm. (Trempe-Graus Basin) - Arro & Fosado (Ainsa Basin)	- Fluvio-deltaic system - Turbidite systems	Nijman and Nio, 1975; Marzo et al., 1988; Mutti et al., 1988; Nijman, 1998; Poyatos-Moré, 2014
Ypresian (upper)	- Perarrua Fm. - Capella Fm.	- Near-shore Sandstones - Tidally fluvio-deltaic system	Nijman and Nio, 1975; Cuevas-Gozalo et al., 1985; Crumeyrolle, 1987

Cuisian)/	- Campanue & Santa Liestra-	Alluvial fans	
Lutietian	Fm.		

ACCEPTED MANUSCRIPT

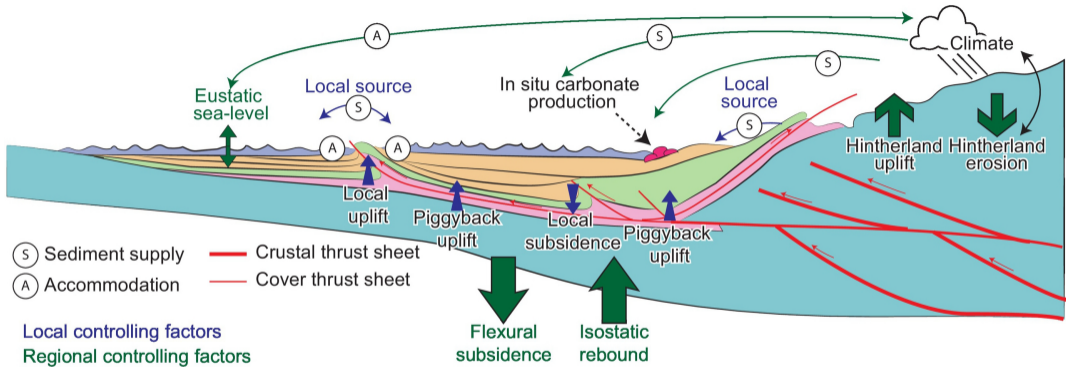


Figure 1

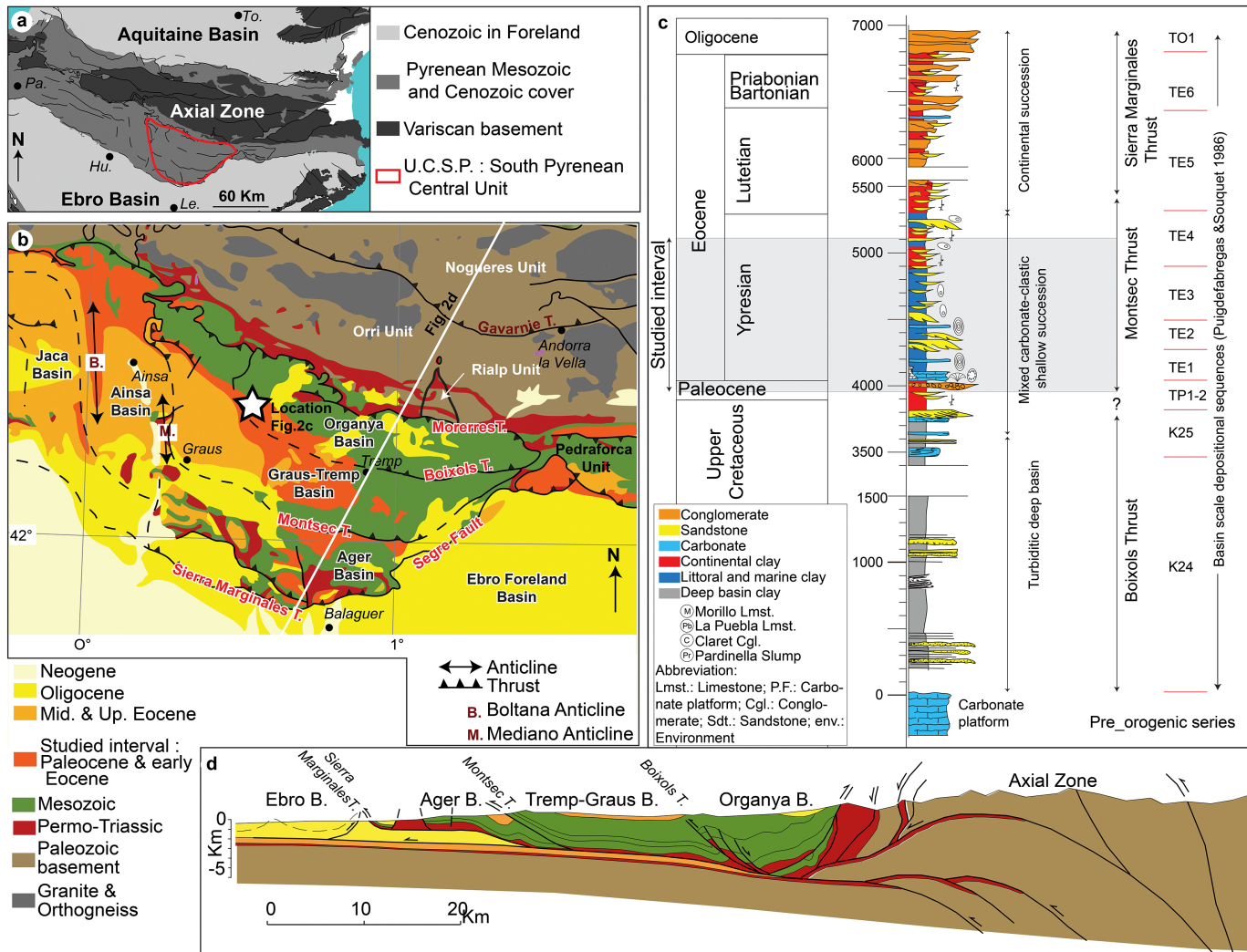


Figure 2

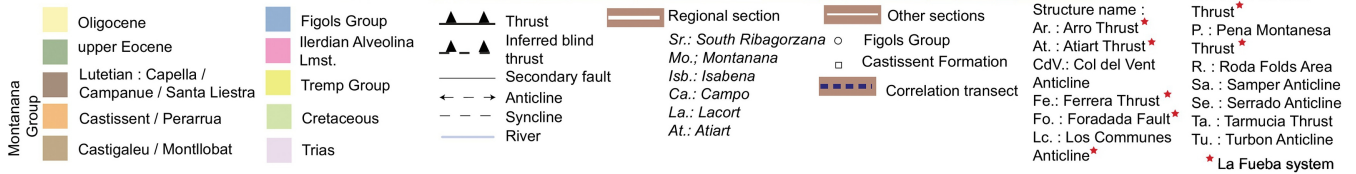
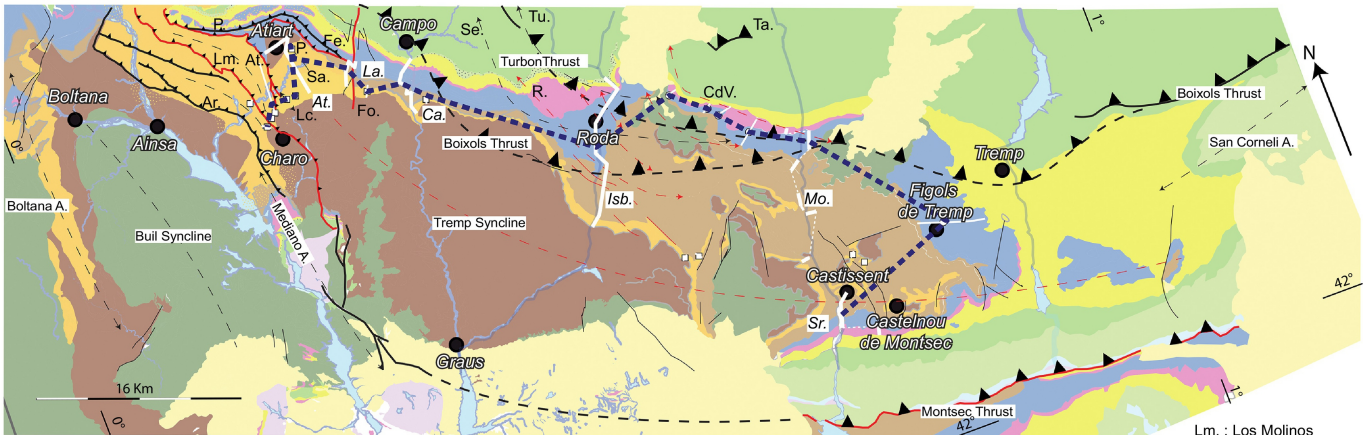
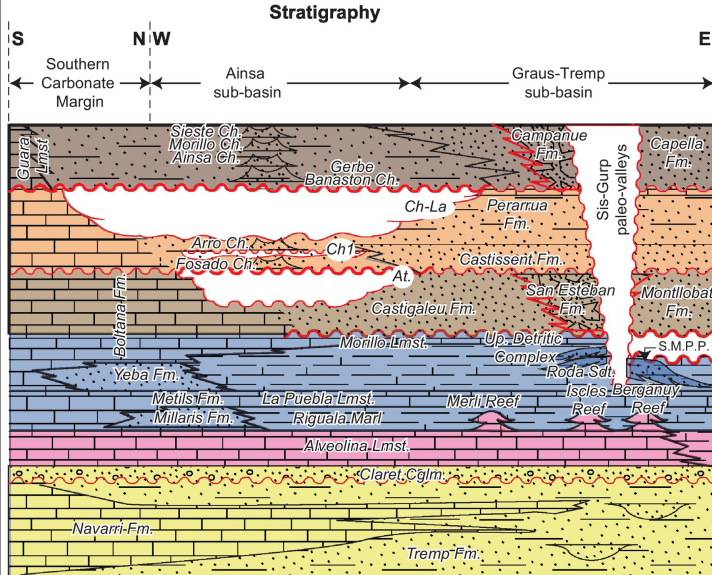


Figure 3

Pujolfabregas and Souquet (1986)		Serra-Kiel et al., (1994) Einhenseer and Luterbacher (1992) Nijman (1998)		Age (Ma)	Period	Epoch	Stage	Geomagnetic Polarity	Planktonic	Larger Benthic	Foraminifers	
Trempe Fm.		Serraduy									Calcareous	Nannofossils
TP 1-2	Trempe Fm.	Serraduy	Alv. Lmst.	56	Paleocene	Thanetian	r	C25	P4	SBZ3	NP7	CP6
				57								
TE1	Figosil Group	Alinya	Llimiana	55	Eocene	Ilerdian	r	C24	P6a	SBZ6/5	NP9	CP8
				54								
TE2	Figosil Group	Alinya	Llimiana	53	Eocene	Ilerdian	p	C24	P6b	SBZ8	NP11	CP9
				52								
TE3	Montanyana Group	Low.	LLM	51	Eocene	Ypresian	p	C23	P7	SBZ10	NP12	CP10
				50								
TE4	Montanyana Group	Mid.	ULM	49	Eocene	Cuisian	r	C22	P8	SBZ12	NP14	CP12
				48								
	Montanyana Group	Up.	UM-B	47	Eocene	Lutetian	p	C21	P9	SBZ13	NP15	CP13
				46								



Tectonic events
(Fernandez et al., 2012
Munoz et al., 2013)

1st. event of rotation in Ainsa basin
 Mediano A.
 Los Molinos Th.
 Atiart Th.
 Foradada Fault
 Roda Folds
 Montsec Th.
 Sierra Marginales Th.

Figure 4

Facies association	Descriptions				Interpretations		
	Lithology and texture	Content and bioturbations	Sedimentary structures and contacts	Depositional sequence organization	Depositional process	Depositional environment	
FA1	- Poorly sorted and sub-rounded pebble-cobble conglomerate supported by a coarse grained sandstone matrix. - Intercalation of very coarse to medium grained poorly sorted sandstones with sharp contact		 Base contact	 6m 0m	- Mass-flows from high-density gravity flash-discharge event - Bedload unidirectional waning flow	Stream-flow dominated alluvial fan	
FA2	- Very coarse to medium grained poorly sorted sandstone with floating pebbles. - Intercalations of conglomerates		 Top contact Base contact	 10m 0m st FS CS Cg	- Unidirectional bedload current during waning floods event. - unconfined flow during late stage of channel filling (plane parallel lamination)	Braided channel	
Three sub-associations							
Geometry		Width/thickness ratio	Sand connectivity	Pelitic facies preservation	Vertical stability	Lateral avulsion	Sub-environment
High horizontal extension Sheet shaped body		>100	High	Low	Low	Strong	Multistorey braided belt channels
Medium horizontal extension Sheet shaped body		50 to 100	Low	Good	Intermediate	Intermediate	Intermediate sheet-like bodies
Low horizontal extension Lenticular body with (1) thick concave-up central body and (2) thin laterally thin «wings»		3:1 to 15:1	Low	High	Strong	Low	Ribbon braided channel
FA3	- Coarse to medium grained sandstones alternated with silty-claystone interval		 Top contact Base contact	 10m 0m st FS CS Cg	- Unidirectional bedload alternation with fall-out suspension - Fluctuation in flow events during a waning flood discharge in high sinuosity channel	Meandering channel	
FA4	- Brownish or reddish silty-claystone - Intercalation of fine to very fine grained sandstone	 	 Top contact Base contact		- Suspension fall out after fluvial food event, channel abandonment or avulsion - channel overbank or crevasse-splays deposits - Paleosols development.	Alluvial plain	
Littoral domain							
FA5	- Very coarse to medium grained sandstone poorly sorted - silty-claystone	 - Oyster, Gastropods fragments - Ophiomorpha	 Top contact Base contact	 5m 0m st FS CS	- Waning stage of flood event - Bedload transport - Overbank deposits	Deltaic plain with subaqueous distributary channel	
FA6	- Bluish gray silty-claystone - Intercalations of decimeters: - (1) marly medium to coarse sandstones - (2) medium sandstone - (3) fine to medium grained sandstones	 - Oysters, Pectens - Ophiomorpha, Skolithos, Cruziana - Thalassinoides - Septaria	Bed (2) Bed (3) Base contact	 2m (1) (2) (3) 0m st FS MS	- Suspension fall out - Brackish, and nutrient-rich waters, variable salinity - (1) Storm deposits - (2) Tidal deposits - (3) Crevasse splay	Bay environment	
FA7	- Coarse to medium grained sandstones intercalated with silty-claystone	 - Broken mollusc shells, - Skolithos and Thalassinoides	 Top contact Base contact	 4m 0 st FS CS	- Lateral accretion in a point bar - Tide current - Draping by marls during periods of tidal slackwater	Estuarine channel	
Legends							
Sedimentary structure			Surface	Sequence organization	Others		
	Trough cross-bedding			Erosive surface		Fining upward	
	Oblique tangential parallel bedding (2D megaripple)			Scours marks		Coarsening upward	
	Horizontal planar bedding			Pebble lag		Thinning upward	
	Current ripple bedding			Mud-clast lag		Thickening upward	
	Climbing ripple bedding			Transitional contact			
	Laterally accreted stratification			Sharp contact			
				Load surface			
						Plants debris	
						Remobilized coal	
						Pedogenesis	
						Mudclast	
						Carbonate nodule	
						Inverse current direction	

Figure 5r1


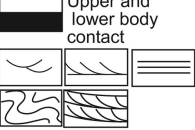
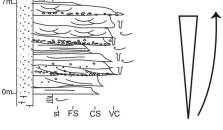
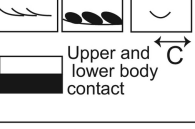
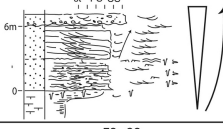

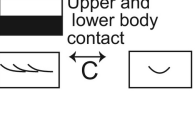


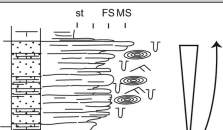

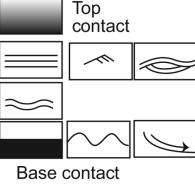
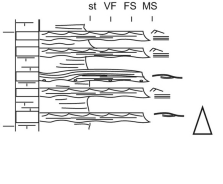
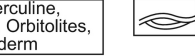


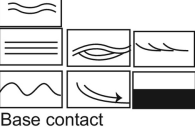


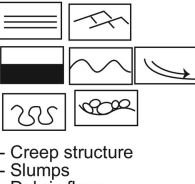
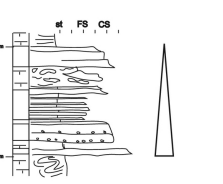
Facies association	Descriptions				Interpretations	
	Lithology and texture	Content and bioturbations	Sedimentary structures and contacts	Depositional sequence organization	Depositional process	Depositional environment
Littoral domain (continued)						
FA8	FA8.1 - Fine to coarse moderately sorted sandstone	 - Gasteropod, Pecten, Oyster - Ophiomorpha, Thalassinoides, Skolithos	 Upper and lower body contact		- Stream-flood events - Unidirectional below	Fluvial dominated delta front
	FA8.2 - Fine to coarse moderately sorted sandstone - Gray silty-claystone intercalation		 Upper and lower body contact		- Stream-flood events - Unidirectional below - Remobilization by tide currents	Fluvial dominated delta front with tide influence
FA9	- Coarse to fine grained sandstones moderately sorted	 - Shells fragments - Nummulitids, Alveolina - Thalassinoides, Skolithos and Ophiomorpha ichnofacies	 Upper and lower body contact		- Subtidal current	Subtidal bar
FA10	- Limestone with Wackstone to grainstone texture - Marls intercalation	- Sandy fraction, - Miliolids, Alveolina, Orbitolite, green algae, oyster, gastropods. - Lucina in marls	- Nodular wavy bedding		- Carbonate production under high energy conditions with well oxygenated water alternated with quiet environment	Inner carbonate platform
Marine domain						
FA11	- Massif poorly sorted marly silt to medium grained sandstone alternating with marly silty-sandstone	- Shell fragments, Assilina, Nummulitids, Alveolina, plants debris - Ophiomorpha, Skolithos and Thalassinoides ichnofacies	 Top contact			Prodelta
FA12	- Heterolithic facies with silty marls and decimeter bedded very fine to medium grained sandstone	 - Assilina, Nummulitids, Alveolina	 Top contact Base contact		- Unidirectional bedload current occurring during major waning flood event - Low density tractive turbiditic current - Hyperpicnite deposits	Turbiditic shelf
FA13	Limestone with: -(1) Wackstone to boundstone texture -(2) Bindstone texture	- (1) Corals, red algae, Alveolina, Orbitolites - (2) Solenomeris, red algae, Nummulitids, Alveolina.			Bioconstruction under (1) Oligotrophic to mesotrophic and, (2) Mesotrophic conditions	Reef environment
FA14	- Limestone with Wackstone to Packstone texture - Occurrence of marls	- Nummulitids, Operculine, Alveolina, Miliolids, Orbitolites, Oyster and Echinoderm			- Carbonate bioconstruction with storm effects	Mid carbonate platform
FA15	- Silty-claystone alternated with medium to fine grained sandstone beds - Sandy limestone beds with reworked fauna	 - Nummulitids - Skolithos, Planolites, Cruziana, Ophiomorpha	 Base contact		- Suspension fall-out - Storm, tide influences	Offshore environment and outer carbonate platform
FA16	- Marly and laminated silty-claystone - Limestone or sandstone blocks	- Reworked fauna (Alveolina, Nummulitids, Red Algae, and Corals)	- Slumps - Debris flows		- Slump - Gravity processes (mass flows) - Slope destabilization	Slope environment
FA17	- Very coarse to medium grained sandstones intercalated with silty brownish to dark claystone - Fine to medium grained sandstones interbedded with siltstones	 - Paleoduction and Helminthorhaphae	 - Creep structure - Slumps - Debris flows		- High density turbiditic flows caused by high discharge of single flood event (channel) - Fall out and traction processes (crevasse splay or levees) - Instable slope with collapse and suggest a nearby flank canyon destabilization	Turbiditic basin

Figure 5r2

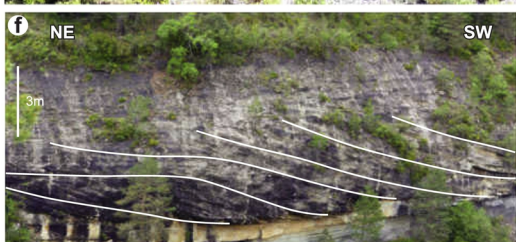
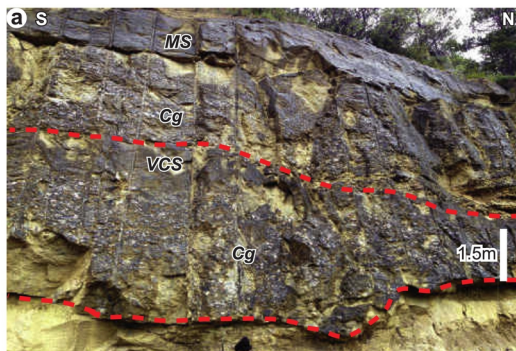


Figure 6ah

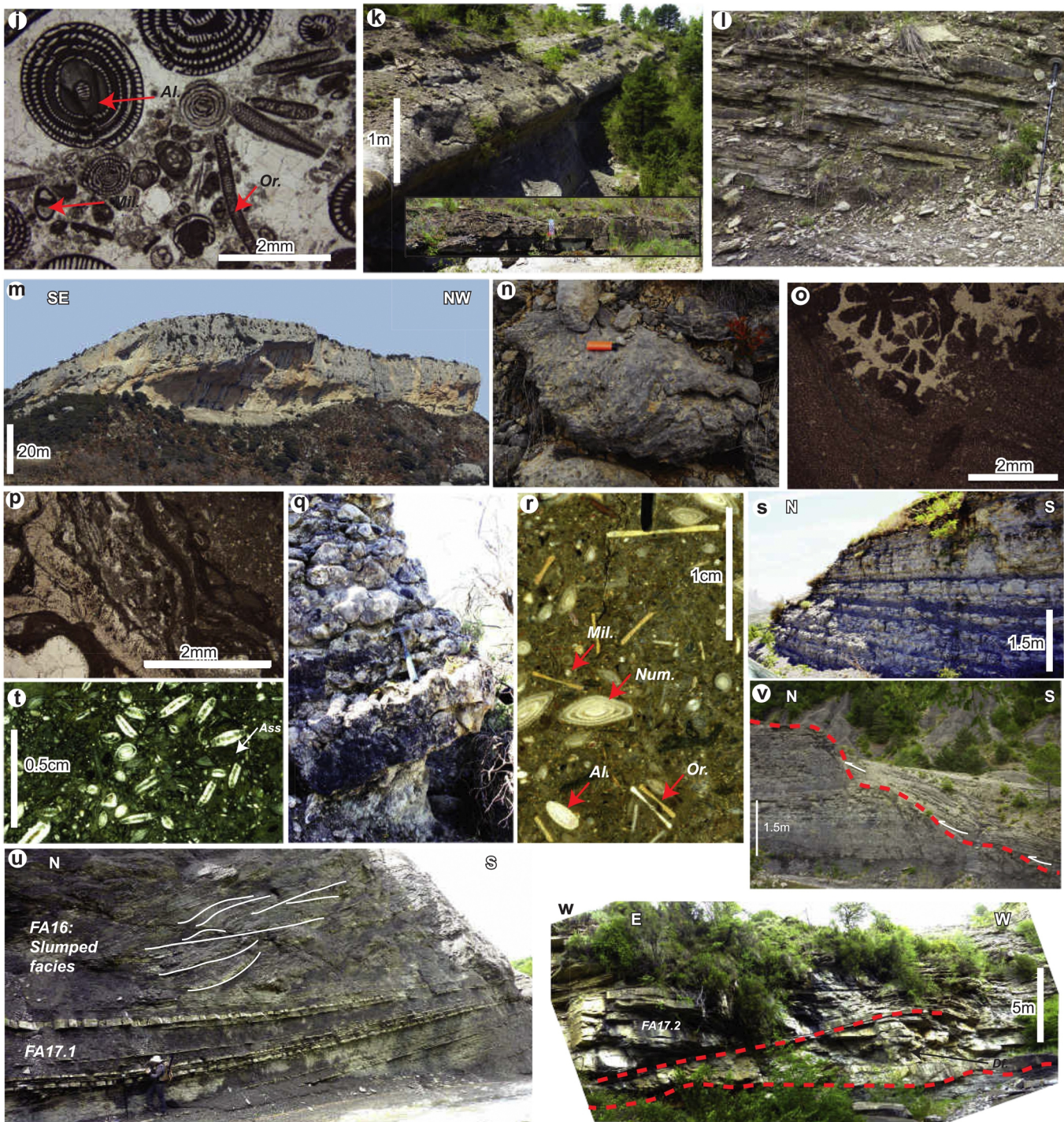


Figure 6jw

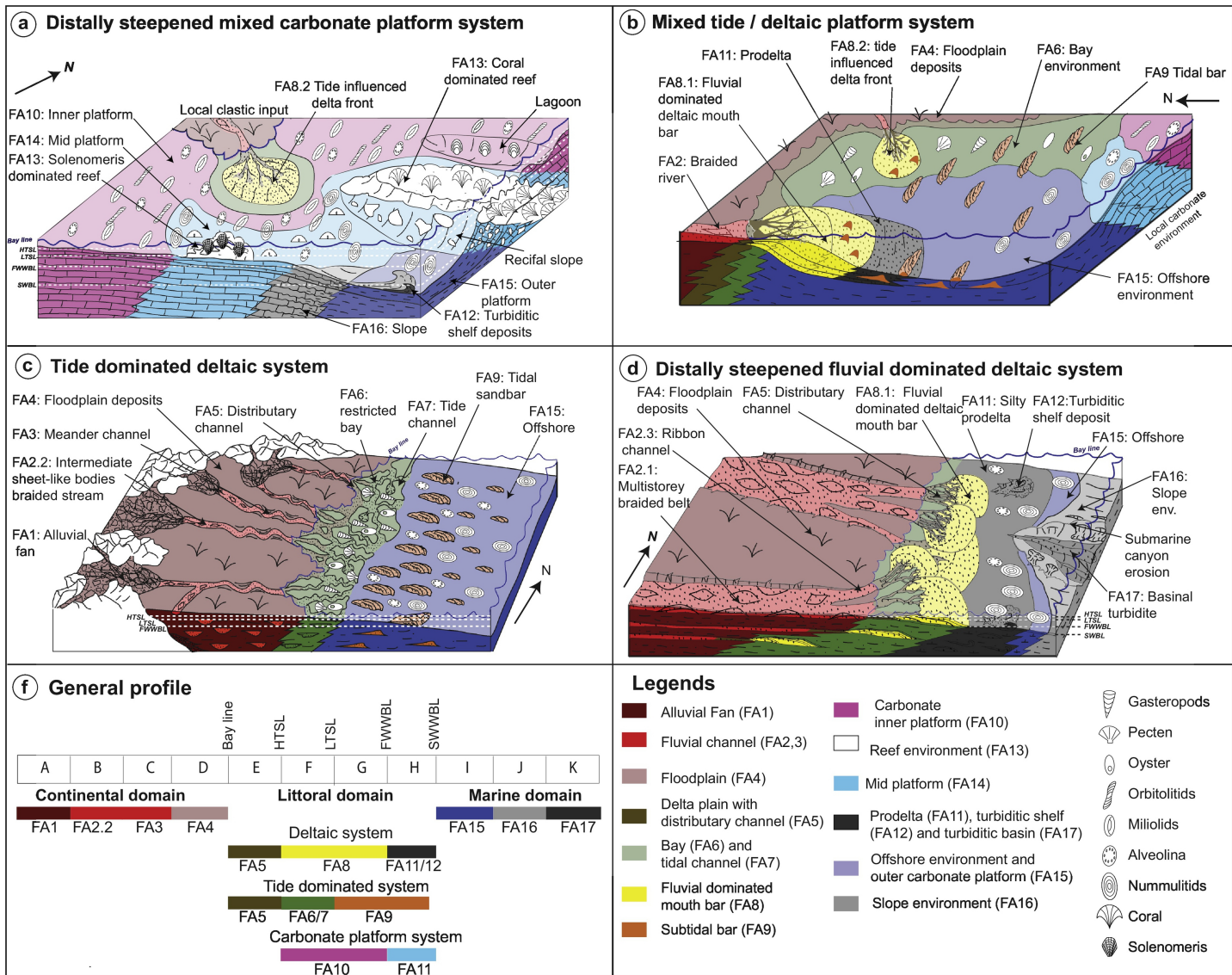


Figure 7

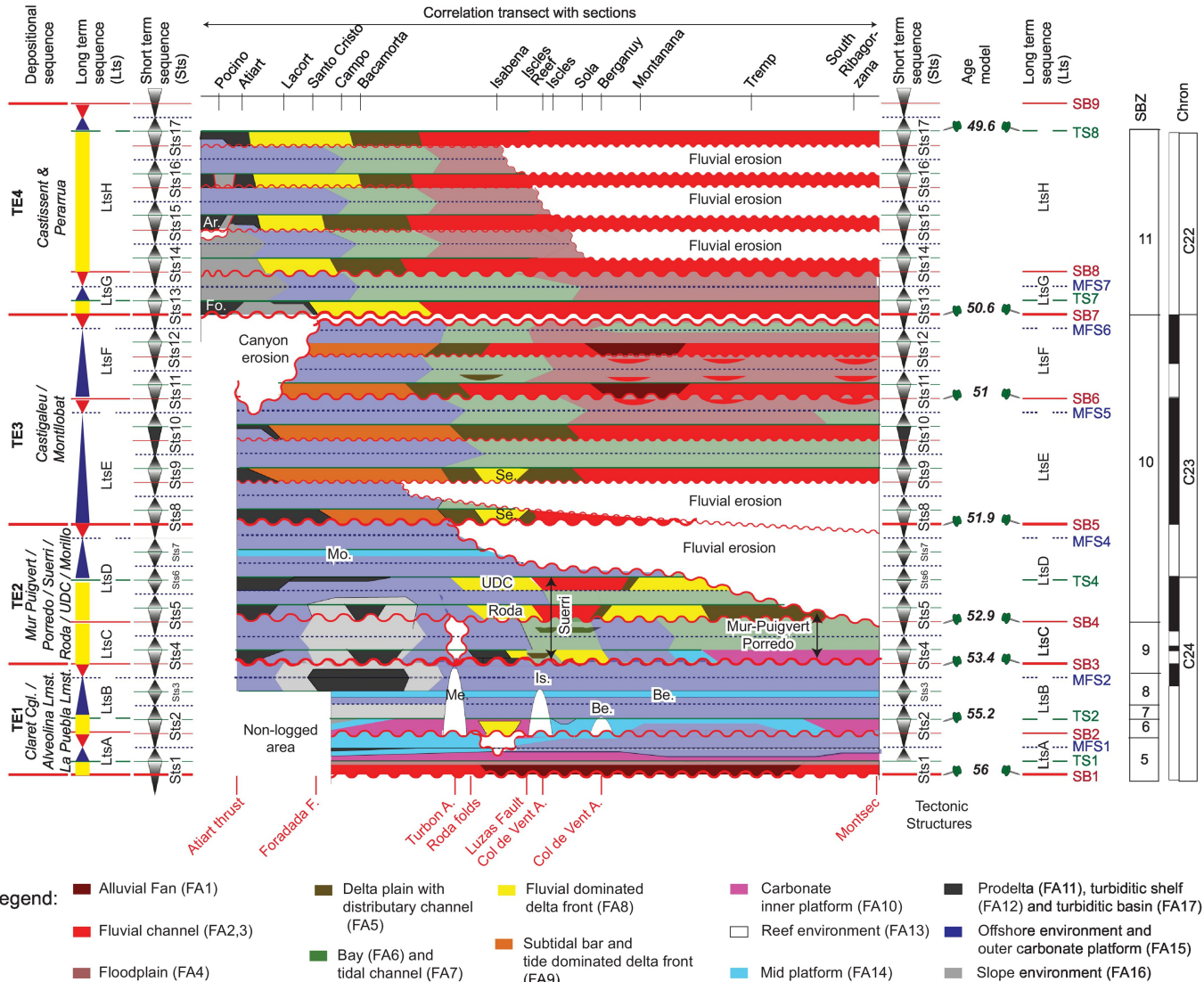


Figure 8

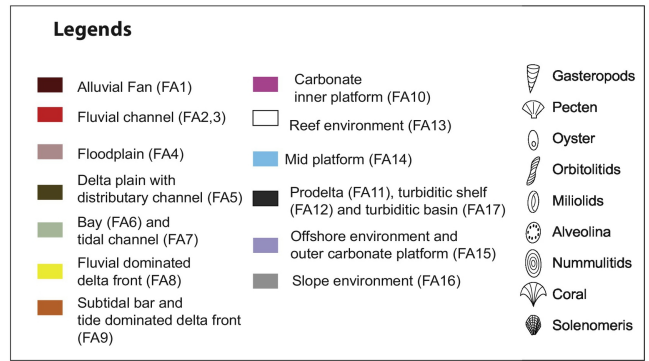
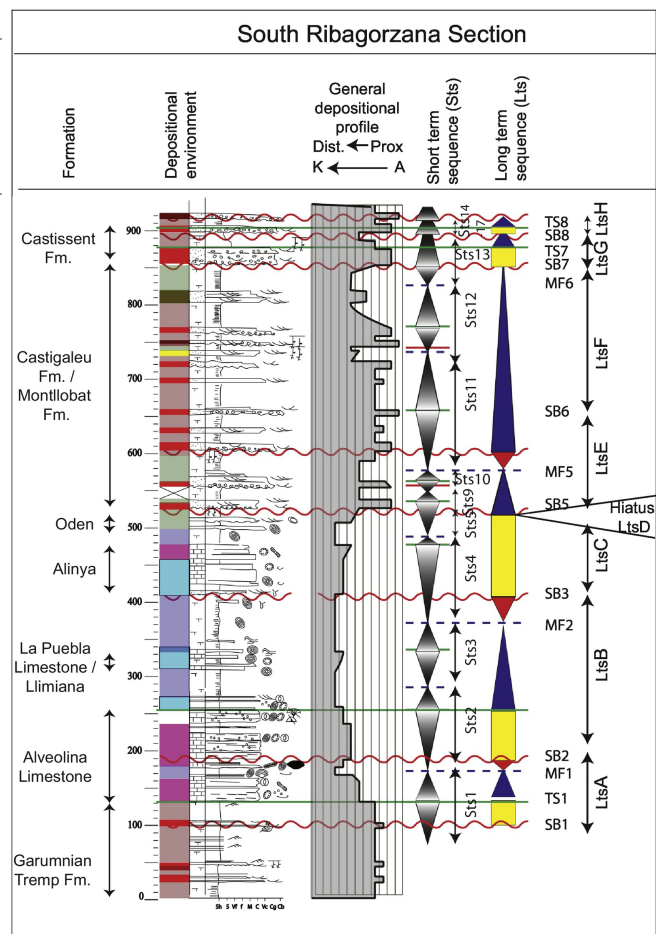
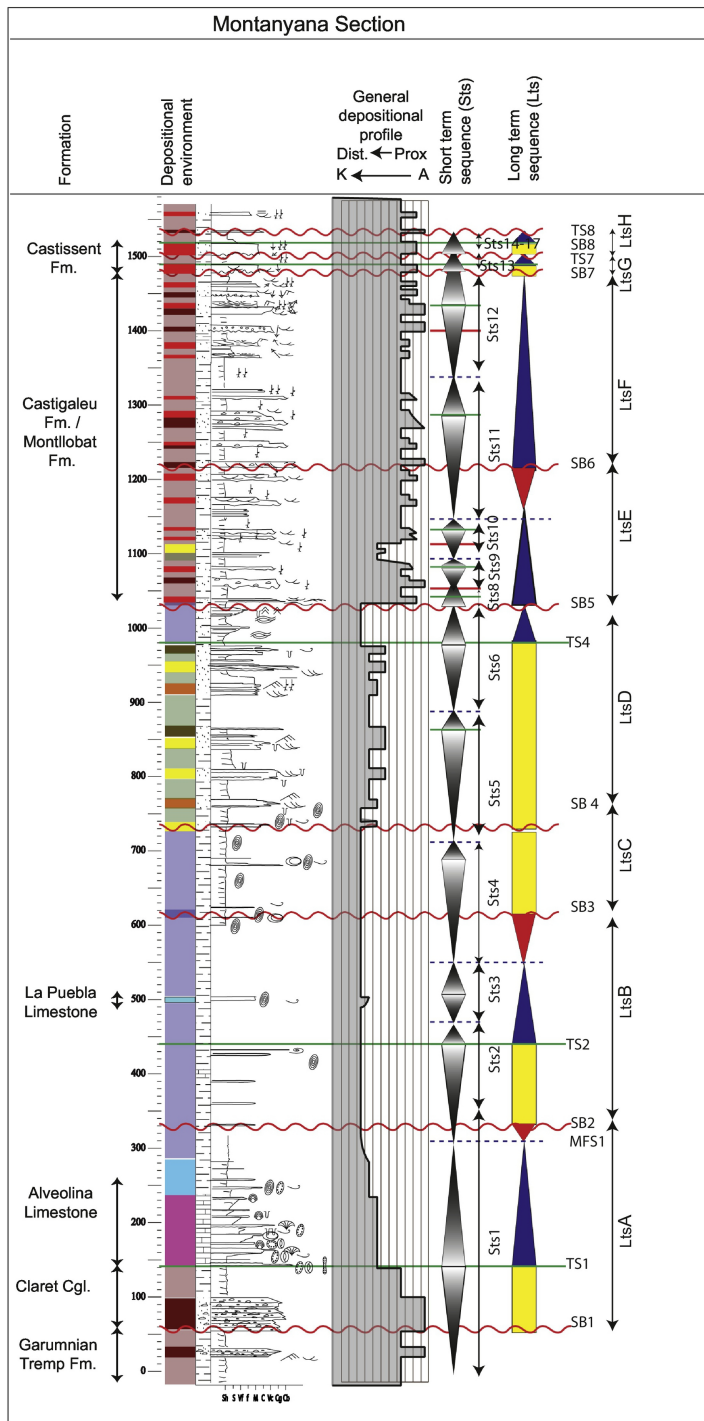


Figure 9

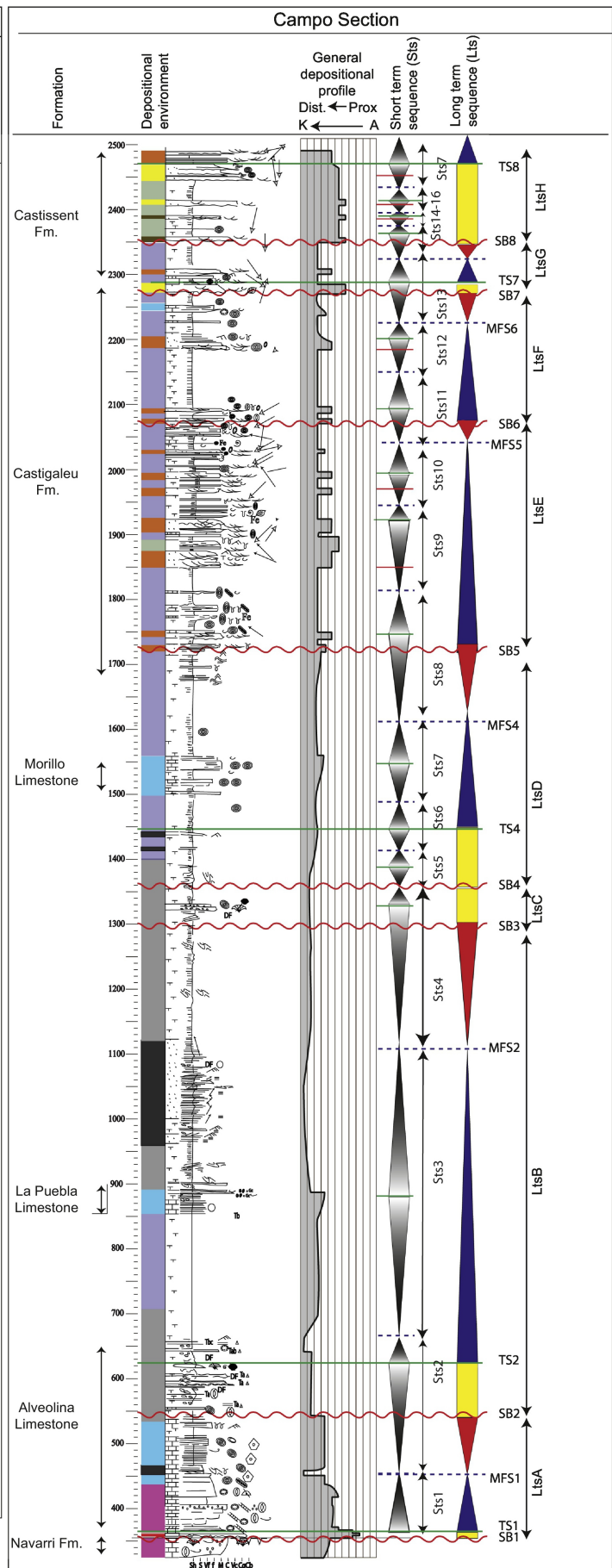
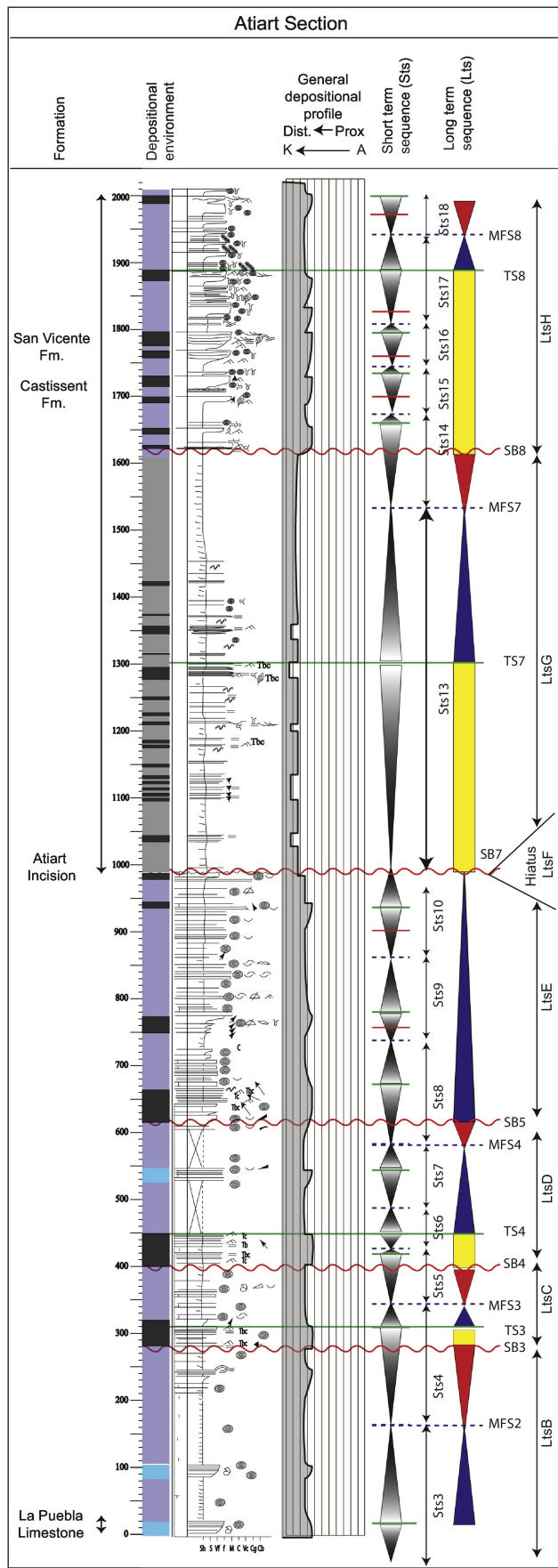


Figure 11

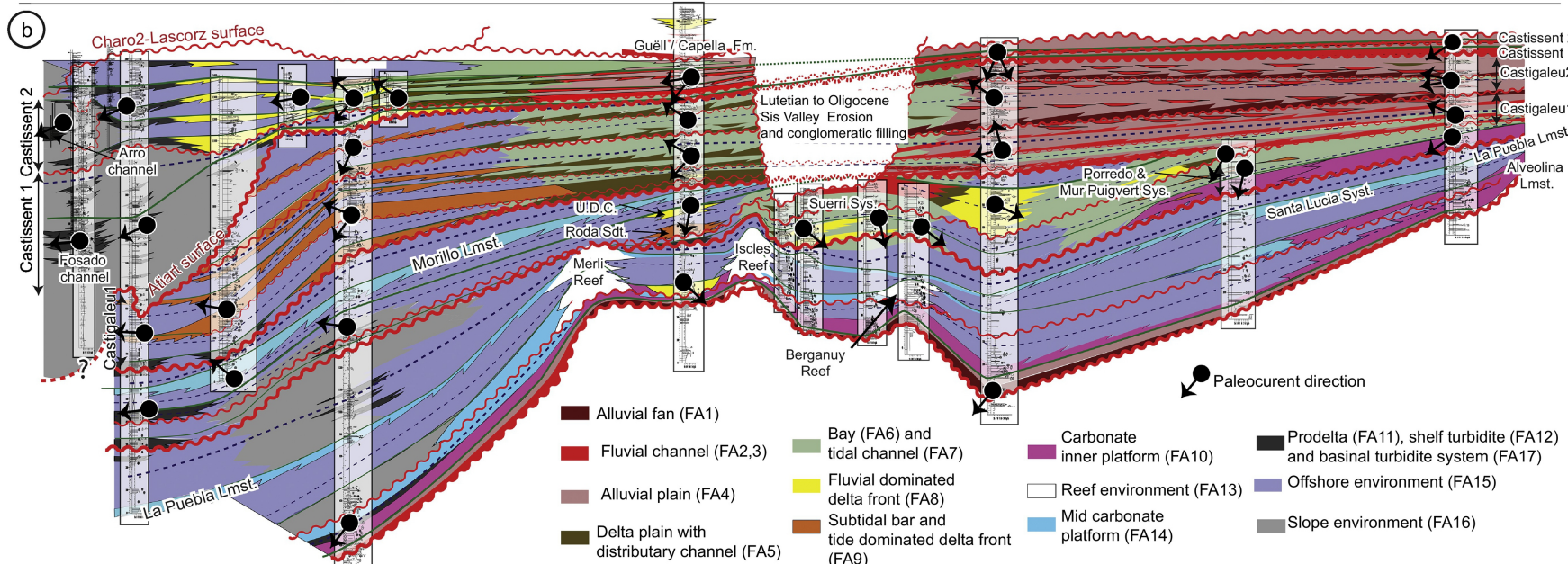
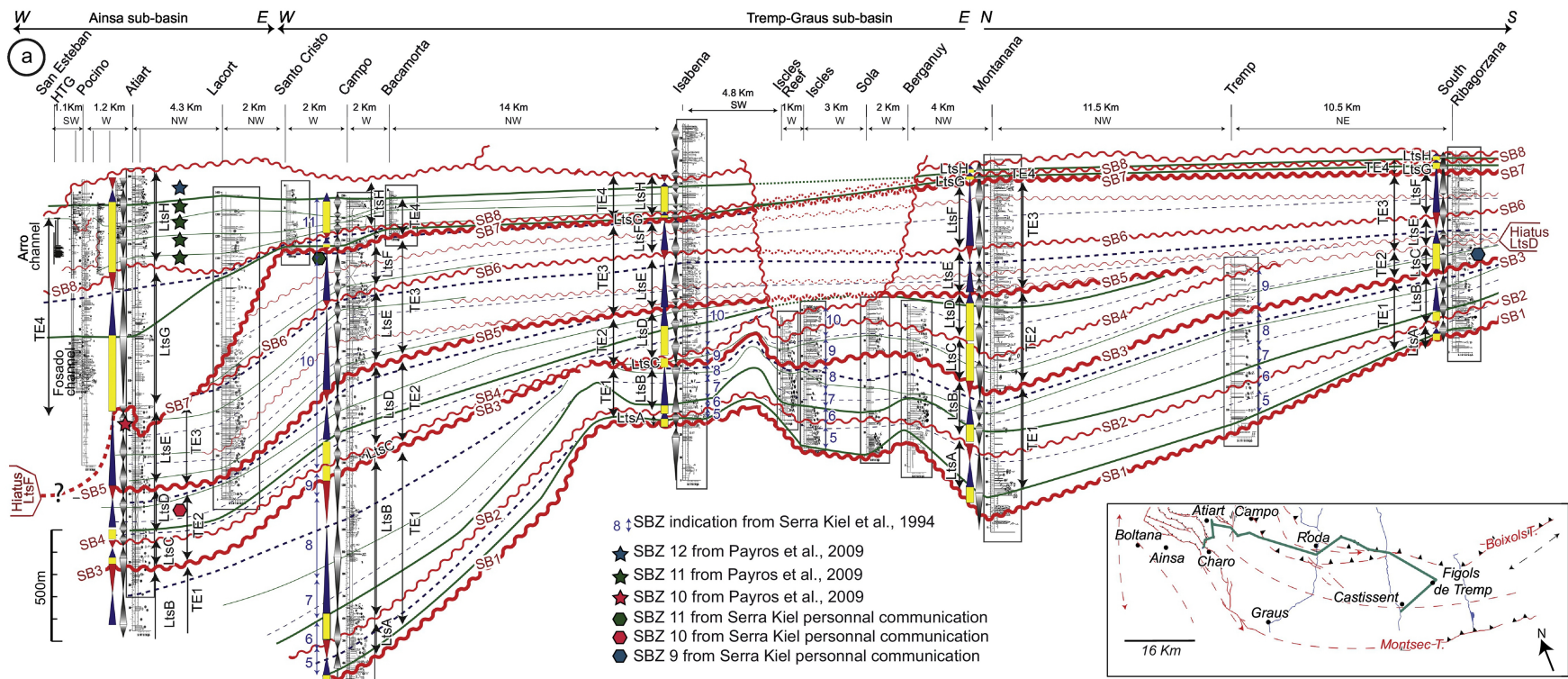


Figure 12

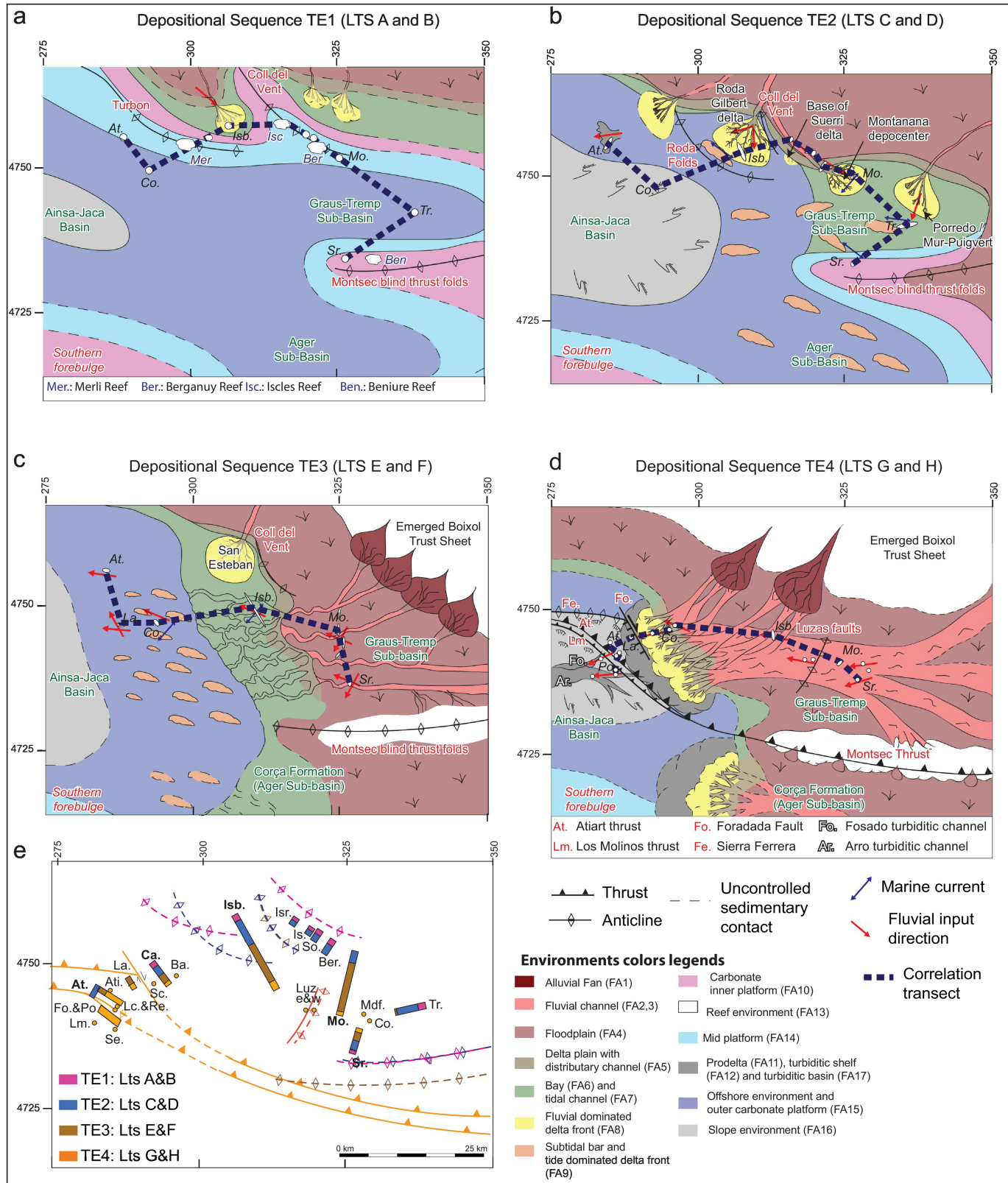


Figure 13

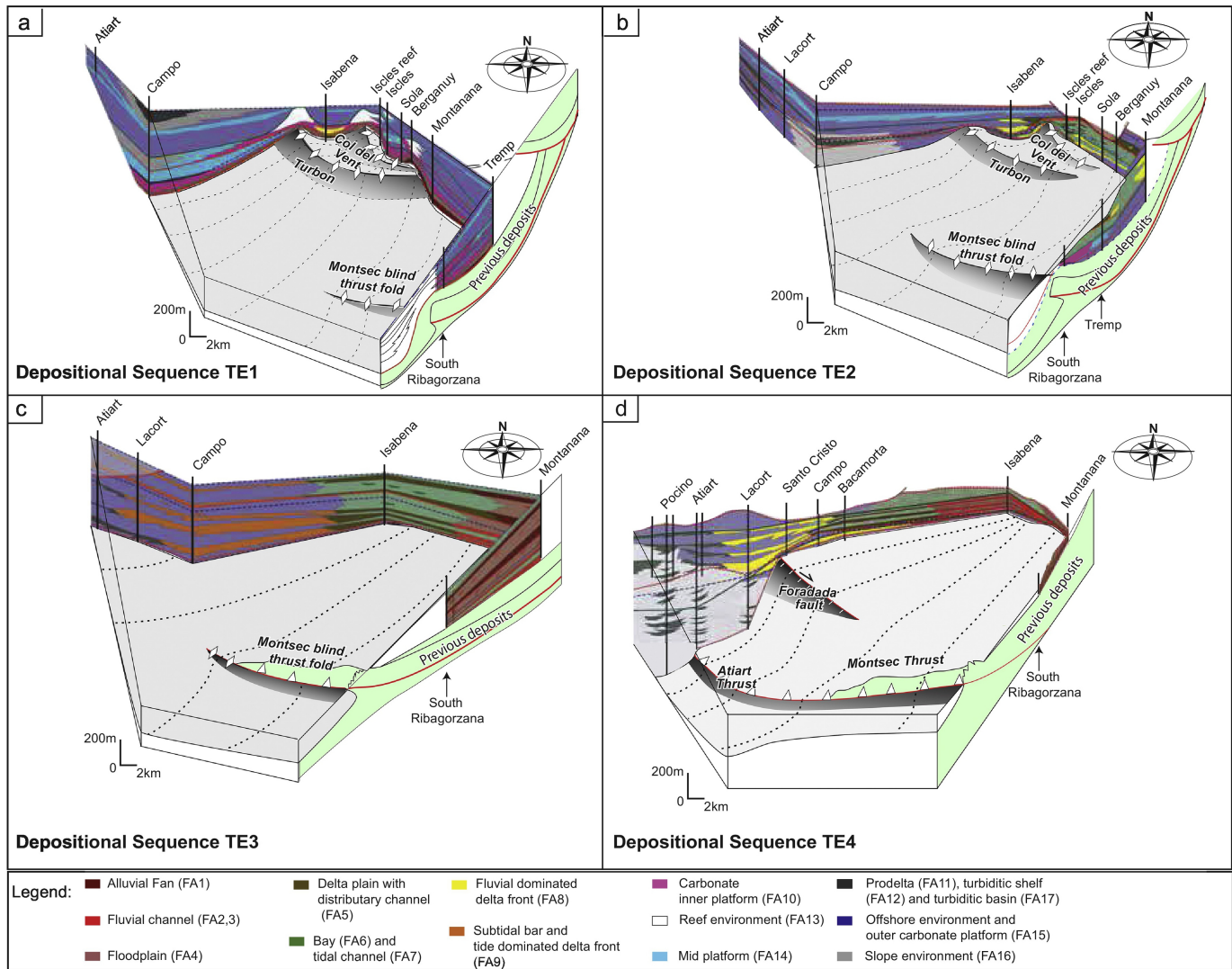


Figure 14

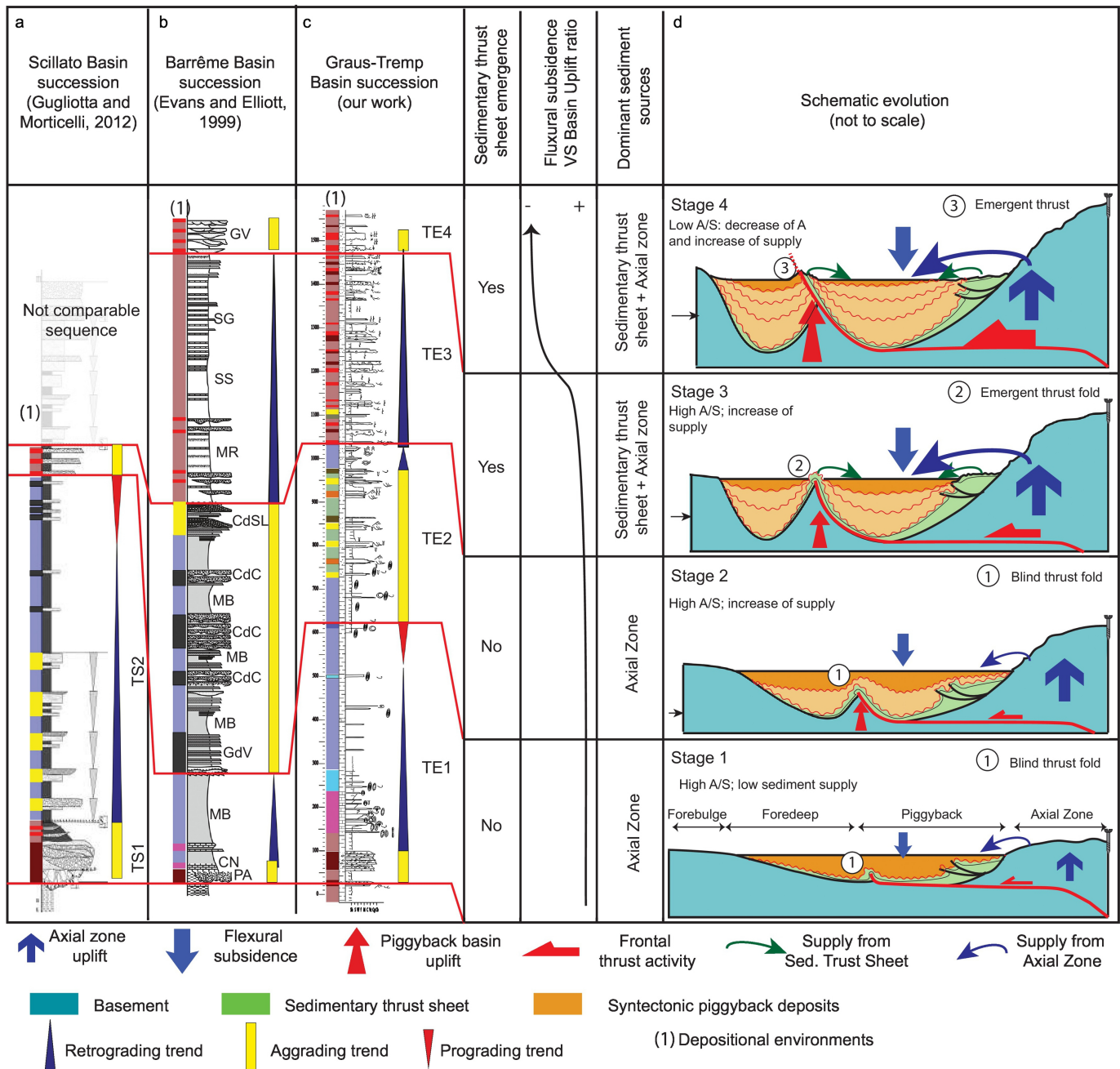


Figure 15